

**Turbulent Characteristics**  
**of**  
**Counter Flowing Wall Jets**

Magdalena Tudor

A Thesis  
  
In  
  
The Department  
of  
Building, Civil, and Environmental Engineering

Presented in Partial Fulfillment  
of the Requirements for  
the Degree of Master of Applied Science  
at Concordia University  
Montreal, Quebec, Canada

December 2003

© Magdalena Tudor, 2003



National Library  
of Canada

Bibliothèque nationale  
du Canada

Acquisitions and  
Bibliographic Services

Acquisitons et  
services bibliographiques

395 Wellington Street  
Ottawa ON K1A 0N4  
Canada

395, rue Wellington  
Ottawa ON K1A 0N4  
Canada

*Your file    Votre référence*

*ISBN: 0-612-91128-4*

*Our file    Notre référence*

*ISBN: 0-612-91128-4*

The author has granted a non-exclusive licence allowing the National Library of Canada to reproduce, loan, distribute or sell copies of this thesis in microform, paper or electronic formats.

L'auteur a accordé une licence non exclusive permettant à la Bibliothèque nationale du Canada de reproduire, prêter, distribuer ou vendre des copies de cette thèse sous la forme de microfiche/film, de reproduction sur papier ou sur format électronique.

The author retains ownership of the copyright in this thesis. Neither the thesis nor substantial extracts from it may be printed or otherwise reproduced without the author's permission.

L'auteur conserve la propriété du droit d'auteur qui protège cette thèse. Ni la thèse ni des extraits substantiels de celle-ci ne doivent être imprimés ou autrement reproduits sans son autorisation.

---

In compliance with the Canadian Privacy Act some supporting forms may have been removed from this dissertation.

Conformément à la loi canadienne sur la protection de la vie privée, quelques formulaires secondaires ont été enlevés de ce manuscrit.

While these forms may be included in the document page count, their removal does not represent any loss of content from the dissertation.

Bien que ces formulaires aient inclus dans la pagination, il n'y aura aucun contenu manquant.

**Canada**

## **ABSTRACT**

### **Turbulent characteristics of counter flowing wall jets**

**Magdalena Tudor**

The industrial effluents and municipal wastewater plant effluents discharged into a stream are expected to undergo dilution in a short reach of the stream. To permit this, the devices used to discharge the effluent should ensure rapid mixing of the effluent in the stream. Jets act as simple and efficient devices that accomplish this task. Counter flowing wall jets located in closed conduits can also be used for efficient mixing of chemicals used in water and wastewater plants.

The increased interest in the use of cross jets and counter flowing jets to ensure proper mixing of effluents in a stream can be traced to the larger scales of mixing achieved by these devices, as compared to the traditional co-flowing jet devices. Existing counter flowing wall jet studies are mostly limited to the determination of the mean flow characteristics of the jet. These include the determination of the functional relationship among the main jet parameters such as the jet velocity ratio, the width of the recirculation zone and the penetration length of the jet.

In the present study, the mean and turbulent mixing characteristics of the counter flowing wall jets were determined experimentally using a Laser Doppler velocity meter (LDA). This information was used to find the dependence of the length scales and the

velocity scales of the counter flowing wall jet on the basic parameters. To validate the experimental procedure, the mean velocity profiles, turbulent components and jet expansion angle of wall jets were determined. The validation was quite good.

In the range of the test covered for counter wall jet, the self-preservation of the mean velocity profiles is approximately in the range  $x/h_j$  from 10 to 40 and is a function of the ratio  $\lambda$  of the jet velocity  $U_j$  to the main flow velocity  $U_M$ . As with other jet flows, the local maximum velocity  $U_m$  and half-width,  $y_{1/2}$  were determined to be the scaling parameters for counter flowing wall jets. An analytical expression is derived for the jet penetration length,  $x_s$ . The jet penetration  $x_s$ , is predicted for various tested  $\lambda$  values.

The measured data related to turbulent characteristics such as turbulent energy balance and turbulent shear stress distributions serve as data banks to validate the results of numerical models simulating counter flow jets.

The above tests were supplemented by studies related to the transport of scalars such as total dissolved solids (TDS) carried by the jet. To this end, surveys of the flow field at selected locations in the jet wake were conducted using a special sampling probe.

A conductivity meter was used to determine the concentration distribution of the TDS (dissolved salt - NaCl) in the jet wake. From individual concentration records at various points at a cross section, the standard deviations of concentration with respect to the section average  $C_{avs}$  were calculated. An empirical relationship between normalized axial distances for total mixing were determined as a function of the velocity ratio  $\lambda$ .

## **ACKNOWLEDGMENT**

The author wishes to thank Dr. A.S. Ramamurthy and Dr. Ngoc Diep Vo for suggesting the research topic. She wishes to express her gratitude to Mr. Lang Vo, Mr. D. Roy, Mr. A. Chociwski and the staff of the machine shop for their contribution during her research years. Finally, but certainly not least, she wishes to express her appreciation to her husband, Petre, for his understanding, encouragements, and support.

## Table of contents

	Page no.
List of Notations	viii
List of Figures	x
List of Tables	xii
<b>Chapter 1     Introduction</b>	<b>1</b>
1.1     Jet - General remarks	1
1.2     Turbulence – general remarks	2
1.3     Dilution – general remarks	5
<b>Chapter 2     Literature review</b>	<b>8</b>
2.1     Turbulent wall jets	8
2.1.1   Existing theoretical and experimental studies	8
2.2     Turbulent counter flowing jets	13
2.2.1   Turbulent counter flowing wall jets	14
2.3     Mixing properties of counter wall jets	15
<b>Chapter 3     Theoretical considerations</b>	<b>18</b>
3.1     Hydrodynamic study	18
3.2     Turbulent quantities	21
3.3     Mixing and dilution	24
<b>Chapter 4     Experimental set-up and Procedure</b>	<b>25</b>
4.1     Experimental set-up and procedure for counter flowing wall jet studies	25

4.2	Equipment and methodology for dilution tests	26
<b>Chapter 5</b>	<b>Analysis of results</b>	<b>27</b>
5.1	Analysis of counter flowing wall jet	27
5.1.1	Velocity distribution	27
5.1.2	Turbulent components	28
5.1.3	Jet expansion	29
5.1.4	Jet penetration	29
5.1.5	Dividing Streamline and Recirculation Zone	30
5.2	Mixing and Dilution	31
5.2.1	Survey of injected TDS concentration using conductivity meter	31
5.2.2	Total mixing	31
5.2.3	Cross flow propagation of injected dissolved solids (salt)	32
<b>Chapter 6</b>	<b>Summary and Conclusions</b>	<b>34</b>
6.1	Summary of results	34
6.2	Suggestions for future studies	35
	<b>References</b>	<b>37</b>
	<b>Appendix</b>	<b>41</b>
	I. Equipment for Flow Measurements	41
	II. Measurement of turbulence with the Laser-Doppler Anemometer	44

## List of Notations

The following notations are used in the present thesis:

$C$	concentration
$C_D$	diffusion constant
$d$	virtual origin location
$h$	width of the returning flow
$h_j$	jet size at $x = 0$
$k$	kinetic energy of turbulence
$N$	number of samples
$Q$	flow discharge
$q$	discharge per unit width
$Re$	Reynolds number
$r_s$	radius where the stagnation S occurs
$U_j$	wall jet velocity
$U_m$	local maximum jet velocity (velocity scale)
$U_M$	free stream (approach flow) velocity
$u, v$	mean velocities
$\bar{u}, \bar{v}$	average mean velocities
$u', v'$	root-mean-squared velocity fluctuations
$u'v'$	shear stress
$x_s$	penetration length from the jet opening to the stagnation point S
$y_m$	location where $U_m$ occurs
$y_{1/2}$	location of the half-maximum velocity (length scale)



$x, y$  stream wise and cross-stream direction

### Subscripts:

$avs$  average of the section

$h_j$  jet opening

$i$  elemental, individual sample

$j$  jet

$m$  maximum

$M$  main

$t$  total

$s$  stagnation

$1/2$  position where mean velocity is one-half the maximum velocity

$0,1$  limit of  $C/C_{avs} = 0$  and  $C/C_{avs} = 1$

### Special Symbols:

$\alpha$  jet expansion angle

$\tau_t$  total shear stress (laminar and turbulent)

$\delta$  boundary layer thickness

$\lambda$  ration of jet velocity,  $U_j$  to free stream velocity,  $U_M$

$\varepsilon$  dissipation term

$\sigma$  standard deviation

**List of figures**

Fig. 1.1a	Definition sketch of wall jet	48
Fig. 1.1b	Definition sketch of counter flowing wall jet	
Fig. 1.2a	Sketch of boundary layer on a flat plate	49
Fig. 1.2b	Turbulent fluctuation	
Fig. 2.1	Definition sketch of plane turbulent wall jet	50
Fig. 3.1	Combination of source and uniform flow	51
Fig. 3.2	Sketch of the dividing streamline and recirculation zone	52
Fig. 4.1	Experimental set-up for counter flowing wall jet	53
Fig. 4.1a	Traverse monitor (left side) and PDA monitor (right side) in front of test section	54
Fig. 4.2	Sampling rake arrangement (cross-section)	55
Fig. 5.1	Velocity distribution of plane wall jet	56
Fig. 5.2	Velocity distribution of the counter flowing wall jet with a wake visualization	57
Fig. 5.3	Mean velocity profile for a wall jet ( $U_M = 0$ )	58
Fig. 5.4	Velocity distribution for $\lambda = 5.105$ , $h_j = 12.7$ mm	59
Fig. 5.5	Turbulent shear stress profiles for plane wall jet	60
Fig. 5.6	Velocity, shear stress and kinetic energy distribution for $\lambda = 5.105$ , $h_j = 12.7$ mm	61
Fig. 5.7	Turbulent kinetic energy for a wall jets	60
Fig. 5.8	Turbulent energy balance of a wall jet	62

Fig. 5.9	Turbulent energy balance for counter flowing wall jet	62
Fig. 5.10	Growth of the length scale for the wall jets	63
Fig. 5.11	Jet expansion for $\lambda$ values	63
Fig. 5.12	Variation of $x_s/h_j$ with $\lambda^2$	64
Fig. 5.13	Dividing streamline geometry	65
Fig. 5.14	Variation of $h/h_j$ with $\lambda^2$	
Fig. 5.15	Recirculation zone	66
Fig. 5.16	Cross-section concentration for $\lambda = 7.6$ at $x/h_j = -64$ in jet wake	
Fig. 5.17	Total mixing distance as function of $\lambda$	67
Fig. 5.18	Limit [1] and limit [0] as function of $\lambda$	
Fig. A1	Optical configuration of typical LDA	68
Fig. A2	Typical velocity signal from individually arriving particles	69
Fig. A3	abcd = area of influence for sampling point 8	70
Fig. A4	Typical plot of standard deviation of $C/C_{avs}$ versus $x/x_s$	71

**List of tables**

Table 2.1	Wall jets studies	72
Table 2.2	Counter flowing studies	76
Table 5.1	Velocity distribution of plane wall jet	77
Table 5.2	Velocity distribution of counter flowing wall jet	82
Table 5.3	Mean velocity profile for a wall jet	91
Table 5.4	Velocity distribution for $\lambda = 5.105$	92
Table 5.5	Turbulent shear stress profiles for plane wall jet	
Table 5.6	Mean velocity, shear stress and kinetic energy for counter flowing wall jet	93
Table 5.7	Turbulent kinetic energy for wall jets	94
Table 5.8	Turbulent energy balance of a plane wall jet	95
Table 5.9	Turbulent energy balance terms of counter flowing wall jet	96
Table 5.10	Growth of the length scale for the wall jets	
Table 5.11	Jet expansion	97
Table 5.12	Variation of $x_s/h_j$ with $\lambda^2$	98
Table 5.13	Dividing Streamline Geometry	
Table 5.14	Variation of $h/h_j$ with $\lambda^2$	99
Table 5.15	Recirculation zone	
Table 5.16	Cross-section concentration for $\lambda=7.6$ at $x/h_j = -64$	101
Table A4	$\sigma$ versus $x/x_s$	101

## CHAPTER 1

### Introduction

#### 1.1 Jets - General remarks

The common modes of jet flows generally include the free jet, the plane wall jet, the cross jet, the three-dimensional jet, the radial and the annular jet. The radial and the annular jets are the less commonly encountered jets.

The wall jet is bounded on one side by a wall. This is a *combination* of two flows that include a free turbulence region in the outer region and boundary layer region near the wall (Schlichting, 2000). There is a strong interaction between these two regions, which forms a complex flow (Fig.1.1a).

The large number of practical problems where we find their application reflects the interest in the plane wall jet flows. These include ventilation, heating (heat treatment of glass or metal plates) and cooling or drying film cooling of the lining walls of gas-turbine combustion chambers.

The counter flowing jets can be classified mainly as circular and plane jets, in which the former are axisymmetric. The counter flowing wall jet (Fig.1.1b) is asymmetric.

The turbulent characteristics of counter flowing wall jets find applications in the process of diluting industrial effluents into a stream (intense mixing), efficient mixing of chemicals in water and wastewater plants (in open channels and closed conduits) and in the design of industrial burners where the air fuel mixture is efficiently mixed using counter jet devices.

The increased interest in the use of cross jets and counter flowing jets to ensure proper mixing in natural streams and treatment plants can be traced to the larger scale mixing achieved by the counter flowing jet devices compared to the traditional co-flowing jet devices. Existing counter flowing wall jet studies are mostly limited to the determination of the mean flow characteristics of these jets. These include the establishment of the functional relationship among the main jet parameters including the geometry of the dividing streamline, the width of return flow and the depth of penetration of the jet.

In the present study, some of the mean and turbulent flow characteristics of the counter flowing wall jets are determined. This information is used to find the relation between the length scales and velocity scales of the counter flowing wall jet and the energy balance terms of the turbulent jet flow field. Surveys of the flow field at selected locations in the jet wake are conducted, using a special design sampler and a conductivity meter to determine the salt concentration distributions in the mixing region of the jet. This yields a measure of the distance at which the injected matter through the counter flowing wall jet is expected to be thoroughly mixed.

## **1.2 Turbulence - General remarks**

Turbulent flow appears random in time and space, and it is not experimentally reproducible in detail (Mathieu, 2000).

Statistical description of turbulence:

1. Mean flow velocity is defined as the average of the velocity over a large number of samples (ensemble average) or as the time averaged velocity;

2. Velocity fluctuation is identified as turbulence;
3. For turbulent flow, mean quantities can be defined. Here, steady means that its statistical properties are independent of time; i.e. the flow is a stationary process.
4. Turbulent characteristics are time and space dependent.

The Reynolds number of the flow characterizes flow instability. It increases with streamwise distance. The random nature of the flow is easily observed using, for instance, a hot-wire or a Laser-Doppler Anemometer (LDA). Such probes produce signals (random velocity fluctuations). The large scales are often evident in the overall fluctuations seen in a graph of velocity versus spatial position or time. The characteristic length scale  $L$ , for correlation length, provides an important measure of the distance over which the velocity fluctuations differ significantly and hence denote the size of the large scales of turbulence.

The turbulent Reynolds number is defined as

$$Re_L = u' L / \nu \quad (1.1)$$

where  $u'$  characterizes the overall velocity fluctuations ( $u'$  is usually taken as the root-mean-squared velocity fluctuation of one of the components of the velocity) and  $L$  is a length scale representing the order of size of the large scales (e.g. a correlation length). The quantities  $u'$  and  $L$ , and hence the turbulent Reynolds numbers,  $Re_L$ , are characteristics of the large scales of turbulence.  $Re_L$  is typically high for turbulent flows, implying little direct effect of viscosity on the large scales; this does not mean that viscosity can be neglected. Viscous effects play an important role in the dynamics of the smallest scales. Dissipation is associated with the smallest eddies. The size of the large

scales is typically fixed by the overall geometry of the flow, for example, the width of a turbulent jet, whereas that of the smallest ones adjusts themselves according to viscosity.

Turbulent flow is rotational, that is, it contains vorticity (twice the rotation). The vorticity is defined as the curl of the velocity,

$$\xi = \nabla \times U \quad (1.2)$$

and thus involves its spatial derivatives. The smallest scales of turbulence, at which the velocity field appears as smooth, dominate the velocity derivatives. These scales are known as the Kolmogorov length scales. Viscosity, which has little influence on larger scales at high  $Re_L$ , is important at the smallest scales. A large Reynolds number is a prerequisite for the production of turbulence. Once turbulent flow is established at high Reynolds numbers, flow instabilities are responsible for continued generation of turbulence, producing large-scale eddies (unstable), giving rise to smaller ones and so on, until viscosity becomes important at the smallest scales. By the cascade process small scales are produced from larger ones, at high Reynolds turbulence. They extract energy from the large scales.

Two-dimensional flow is the one that is independent of the  $z$  direction (lateral direction). The mean velocity  $W$  in that direction is zero. Turbulent flow can nonetheless be two-dimensional in a statistical sense (statistical properties independent of  $z$  with zero mean-velocity component in that direction). However, turbulence in any given realization is three-dimensional.

Turbulence can be symmetric, for instance, developed flow in a plane channel is symmetric with respect to the center plane of the channel as well as being homogeneous. Turbulence is important for combustion, chemical engineering problems, multiphase



flows, meteorology and pollutant dispersal. The flow velocity  $u$  is split into a mean part  $\bar{u}$  and a fluctuating component  $u'$  (representing the turbulence) (Fig. 1.2b). Thus, in the flow direction,

$$u = \bar{u} + u' \quad (1.3)$$

Here,  $u'$  is the fluctuation of velocity interpreting as representing the turbulence. Generally, turbulence intensity in different directions can be measured by the standard deviation

$$u_i' = \left( \overline{u_i'^2} \right)^{1/2} \quad (1.4)$$

Turbulent energy is an important measure of the intensity of turbulence.

Further, turbulent kinetic energy per unit mass

$$\frac{1}{2} \overline{u_i u_i} = \frac{1}{2} \sum_{i=1}^3 \overline{u_i'^2} = \frac{1}{2} \left( \overline{u_1'^2} + \overline{u_2'^2} + \overline{u_3'^2} \right) \quad (1.5)$$

is the most common quantitative measure of the turbulent intensity.

Isotropic turbulence (direction independent) can be adopted to simplify the analysis, for certain turbulent jet flows stated earlier.

### 1.3 Dilution – General remarks

In earlier times, wastewater disposal practices were based on the premise that “the solution to pollution is dilution.” (Peavy, 1985). Dilution in natural water bodies was considered the most economical means of wastewater disposal. Mixing promotes dilution. Turbulent jet mixing can be used as an alternative to mechanical mixing in water treatment plants for mixing disinfectants such as chlorine.

The main challenge faced by engineers is to come up with an efficient configuration where a rapid and thorough mixing can be achieved in a relatively short distance. The optimum mixing distance is usually defined as the distance at which the variation of concentration over the cross-section is some small-specified value (Benzina et al., 1974).

The applications of the counter flowing wall jets increased the interest into diluting industrial effluents in a stream (intense mixing), efficient mixing of chemicals in water and wastewater plants and in the design of burners where the air fuel mixture is efficiently mixed using counter jet devices.

The increased interest in the use of cross jets and counter flowing jets to ensure proper mixing in streams and treatment plant system can be traced to the larger scales of mixing achieved by counter flowing jet devices as compared to the traditional jet devices. While diluting, the amount of solvent is increased, but the amount of solute is kept constant. The result is a decreased concentration, but a greater volume. The idea is that the volumes may change but the number of moles of the solute does not. This means that the original number of moles and the final number of moles are the same.

$$\text{number moles original} = \text{number of moles final}$$

The word descriptions for numbers of moles can be replaced by the molarity and, volume. The difference between the original volume and the final volume yields the amount of solvent needed to make the desired "dilution". Dilution by definition is a process of reducing the concentration of a solute in solution. One achieves this by mixing the solute with more solvent. Dilute solution by definition is a solution that contains a small amount of solute relative to the amount that could dissolve (Volland, 2000).

The dilution capacity of a stream can be calculated using the principles of mass balance. The concentration after mixing can be calculated as follows

$$C_s Q_s + C_w Q_w = Q_m C_m \quad (1.6)$$

Here,  $C$  = concentration (mass/volume) of the matter considered,  $Q$  = volumetric flow rate (volume/time). The subscripts  $s$ ,  $w$ , and  $m$  designate stream, waste and mixture conditions.

## CHAPTER 2

### Literature review

#### 2.1 Turbulent wall jets

##### 2.1.1 Existing theoretical and experimental studies

The plane wall jet was examined theoretically first by Glauert (1956). He has examined the similarity problem of laminar and turbulent jets as well as the similarity in radial and plane wall-jets. He assumed an eddy-viscosity behavior implied by the Blasius one-fourth power friction formula in the boundary layer, and taking it as constant in the free mixing region, developed analytically a velocity distribution which could be made to describe the observed profiles by the proper selection of a parameter. Following the work of Glauert, Schwarz and Cosart (1960), they assumed that the mean and turbulent velocity fields are self-similar. These investigators used the aid of a hot-wire anemometer to examine the velocity profiles in some detail. The Reynolds number based on the maximum velocity and the thickness of the boundary layer was from 22,000 to 106,000. Velocity nozzle speeds were: 27, 40, 60, and 83 ft/sec, with a range of distance downstream of the outlet from 1.5 to 5.5 ft. They found that the location of the virtual origin is a function of the free-stream turbulence in the jet, the wall roughness, vibration, sound, and also the outlet Reynolds number  $Re$ . The angle between the locus of the boundary-layer thickness and the plate has been found to be  $\alpha = 3.8^\circ$ . This compares well with Sigalla's (1958) result for  $\alpha = 3.7^\circ$  ( $20,000 < Re < 50,000$ ).

The ‘law of the wall’ is not applicable to the turbulent wall-jet in the form obtained experimentally in turbulent boundary layers, turbulent pipe and channel flows. In the outer layer of the wall-jet and near the position of maximum velocity, there is a considerable difference in the velocity profile from that of a free jet or a mixing layer.

Verhoff (1963) has also investigated the similarity problem. He found an empirical equation (based on experimental data) to describe the similarity curve of the velocity distribution:

$$u/U_m = 1.48\eta^{1/7}[1 - \text{erf}(0.68\eta)], \quad (2.1)$$

where  $\eta = y/y_{1/2}$ .

Hanjalić and Launder (1972) developed the Reynolds stress model to a thin shear flow and an energy balance in a wall boundary layer. They also obtained the velocity and shear stress profiles predictions in plane wall jet and compared them with Thailand’s experimental data. They compared the energy balance in a plane jet with experiments results of Bradbury (1965).

Ljuboja and Rodi (1980) studied the turbulent wall jets with an algebraic Reynolds stress model (co-flowing and plane wall jet case) using  $k$ - $\epsilon$ , and  $k$ - $\omega$  equations.

Chandrsuda and P. Bradshaw (1981) studied the terms in the turbulent energy and shear stress balance for which the turbulent kinetic energy is defined by Eq (2)

$$k = \frac{1}{2} (u^2 + v^2 + w^2) \quad (2.2)$$

$k$  can be reduced for isotropic cases to the following form

$$k = \frac{3}{4} (u^2 + v^2) \quad (2.3)$$

Gerodimos and So (1997) investigated the near wall modeling (based on the direct numerical simulation (DNS); the  $k$ - $\epsilon$  and  $k$ - $\omega$  models ) of plane turbulent wall jets, for

which they obtained a good agreement with other measured quantities. The models were capable of reproducing the Reynolds number effects on plane wall jets.

Tangermann and Gratler (2001) did a computation of a two-dimensional turbulent wall jet in a co-flowing external stream. The standard  $k-\epsilon$  model and a full Reynolds-stress model have been used for the numerical analysis.

The literature regarding experimental results of wall jet flows is very extensive. The studies should be examined based on the instrumentation utilized to perform the measurements. Early investigations used Pitot tubes to measure the mean velocity profiles, their growth and decay rates. Later hot-wire anemometers were used to measure the turbulence, and the latest investigations are using laser Doppler for turbulent measurement.

The earliest experimental work on the wall-jet in still air was carried out by Förthmann (1934). He based his study on a theoretical paper by Tollmien (1926). Förthmann found that the mean velocity field was self-similar, the half-width ( $y_{1/2}$ ) grew linearly and the maximum velocity inversely proportional to the square root of the stream wise distance. Using Pitot tube he found that the local maximum velocity could normalize the mean velocities profiles.

Sigalla (1958) used a Pitot tube for velocity measurements, and a Preston probe for the measurement of wall shear stress. The boundary layer thickness varied linearly at an angle of  $3.7^\circ$  with the plate, and passing approximately through the center of the outlet nozzle of the jet. The following equation

$$y_{1/2}/h_j = 0.0647(x/h_j + 7.73) \quad (2.4)$$

is the growth rate equation.

Bradshaw and Gee (1960) presented the first turbulence measurements in wall jet, and Schwarz and Cosart (1960) found that the angle between the locus of the boundary-layer thickness and the plate is  $3.8^\circ$ .

Tailland and Mathieu (1963, 1965, 1967) studied the turbulent characteristics of the plane wall jet and the distribution of turbulence production. They found a Reynolds number dependence for the streamwise development of maximum velocity and half-width. They defined characteristic velocity as the maximum speed into a section and as characteristic dimension  $y_{1/2}$  the distance from the wall where the speed becomes half of the maximum local value. It was the first figure plotted using the traditional normalization (1967).

Rajaratnam and Subramanya, (1967b) made observations on the decay of the velocity scale, and also they sketched the various parts of the plane turbulent wall jets (Fig. 2.1). The average curve was described by the following equation

$$U_m/U_j = 3.5/\sqrt{x/h_j}; x/h_j \leq 100 \quad (2.5)$$

The virtual origin is located roughly  $10h_j$  behind the nozzle, and it is described by the equation

$$y_{1/2} = 0.068x \quad (2.6)$$

The first energy balance for the turbulent kinetic energy over a convex surface, assuming isotropy in dissipation was presented by Alcaraz (1977).

A cornerstone in the study of wall-jets is the review of Lauder and Rodi (1981). They studied four cases in the area of a turbulent wall jet: self-preserving 2D wall jet on a plane surface at 50 slot heights downstream of exit slot; plane 2D non-similar wall jets on a plane surface; 2D wall jet on logarithmic spiral surface, and plane 3D wall jet in

stagnant surroundings. Later in 1983, they studied another case for the turbulent wall jet measurement and modeling for the plane two-dimensional co-flowing wall jet; the wall jet on curved surfaces; the radial wall jet and the three-dimensional wall jet. They claim that for the plane two-dimensional wall jet in quiescent surroundings, the linear growth of the half-width was 7.3%, the shear stress was not zero at the point of maximum mean velocity and the interaction of the outer and inner layer attenuated the logarithmic mean velocity profile. The uncertainty of the turbulence data was high (Abrahamsson et al., 1994).

Kobayashi and Fujisawa, 1985 found the growth rate equation of the half width to be

$$y_{1/2}/h_j = 0.066(x/h_j + 10) \quad (2.7)$$

Also, they found an interesting comparison with free jet turbulence measurements.

Schneider (1987) found the same growth rate equation to be

$$y_{1/2}/h_j = 0.077 (x/h_j + 8.7) \quad (2.8)$$

and the decay rate to be  $U_m/U_j = 6.122 (x/h_j + 8.7)^{-0.608}$ . He used the LDA to capture the Reynolds stress, in the outer most region, where the literature based on hot-wire measurements revealed the largest deviations due to the high local turbulence intensity. The normal stresses were found to be slightly larger as compared to hot-wire data.

Fujisawa and Shirai, 1987 investigated the turbulent energy balance in a two-dimensional wall jet along a plane surface, and found that the convection velocities of the small-scale turbulent motion deviated significantly from the mean velocity.

Johansson and Karlsson (1988) used the water tunnel for the wall jet tests and computed the energy budget in the near-wall region of the turbulent boundary layer using



experimental data. The agreement with the energy budget for the boundary layer (Hinze, 1975) was poor. However, their data agreed well with the one from (DNS).

Karlsson (1991, 1993) used the Pitot tube and LDV systems to study the 2D plane turbulent wall jet in water.

In 1994, Abrahamsson et al. used a hot-wire technique in a large scale experimental scale facility and compared their results with LDA measurements, in the self-preserving region between 70 and 175 normalized locations.

Hsiao and Sheu (1996) used the hot-wire techniques in their experimental studies on the flow transition of a plane wall jet.

Eriksson et al. (1998) used both LDV systems and hot-wire techniques. Turbulence data from the outer region of the flow were compared with earlier hot-wire measurements, and large differences in normal turbulent intensity and shear stress were found. George et al. (2000) studied the turbulent plane wall jet without an external stream. Table 2.1 is a summary of the various wall jets studies.

## **2.2 Turbulent counter flowing jets**

Arendt et al. (1956) published the first paper regarding the circular counter flowing free jet (Saghravani, 2002) with only one reference of Albertson et al. (1950). They defined two dimensionless functions based on the jet system geometry and momentum. A Pitot tube measured the velocities. The result showed a linear relation between the penetration length and the velocity ratio as in the following equation

$$X_s / D = 2.4 U_j / U_M \quad (2.9)$$

where  $D$  is the jet diameter. Later Beltaos and Rajaratnam(1973), Konig and Fiedler (1991) and Lam and Chan (1995) show that the results are not valid for all jet velocities although the equation can be used for the velocity ration  $\lambda \leq 10$ . Rajaratnam (1973) used the wind tunnel as the test section with a nozzle mounted in the center to provide the counter flowing jet.

### 2.2.1 Turbulent counter flowing wall jets

Although a large amount of studies exist in the area of jet flows, the characteristics of turbulence in counter flowing jet have not been explored fully (Table 2.2). Existing counter flowing jet studies mostly deal with the mean flow characteristics. In particular, earlier studies were devoted to the determination of the geometrical characteristics of the dividing streamline and the depth of penetration of the counter flowing jet.

Hopkins and Robertson (1967) investigated the two-dimensional incompressible fluid jet penetration with the following characteristics. They noticed the appearance of free streamlines at the sides of the jet and of a dividing streamline, which separates the jet and the penetrated fluid. They used a kinematic analysis via free-streamline theory and the hodograph that has been developed with one unspecified parameter, the ratio of jet to counter stream velocity in the steady flow case.

Robillard and Ramamurthy (1974) studied the vortex street generated by a plane jet in a counter flow. The paper explored the geometric and fluid dynamic parameters associated with the counter jet oscillation, and also studied the near wake characteristics of a counter jet. The oscillation phenomenon was related to a jet Strouhal number. A

vortex shedding mechanism is normally present in centrally mounted two-dimensional free counter flowing jets (Robillard 1974a, 1974b).

Colin (1968), Robillard (1974a,b) and Balachandar et al. (1992) have studied some of the mean flow characteristics of a wall jet beneath a counter flowing stream. Mean flow characteristics of counter flowing wall jets such as the geometrical characteristics of the dividing streamline (DSL). They reported the penetration zone and the wall pressure distributions. The geometric characteristics of a counter wall jet are very similar to that of a free jet in a counter flow. The protrusion above the jet exit did not disturb the flow and the optimum size and shape of the wall jet injection device can be chosen after conducting simple jet interference tests.

Tanaka et al. (1994) conducted an experimental study on the two-dimensional counter flowing wall jet in a turbulent boundary layer. They found the streamlines, turbulence intensity contours and static pressure contours for two typical velocity ratios  $\lambda = U_j/U_M$ . The range of  $\lambda$  was 1 to 3. Recently, the mixing characteristics of turbulent wall jets in cross flows used in stream pollution control have been reported (Rajaratnam, 1995). The increased interest in the use of cross jets and counter flowing jets as devices for the disposal of effluents in a flowing stream can be traced to the larger scales of mixing achieved by these devices compared to the limited mixing scales achieved by traditional co-flowing jet devices.

### **2.3 Mixing properties of counter wall jets**

Turbulent mixing and dispersion of jets in a stagnant ambient and in a moving current are of great importance in environmental hydraulics. Study of many flow situations have

been reported in literature (e.g., Wood 1993 for a review) and among them, the counter flow case had received the least attention (Lam and Chan, 2002). In the 1950s and 1960s, a number of Russian researchers studied the mean flow behavior of a circular jet in a counter flow, with applications in aerodynamics as the key objective (e.g., Sekunkov 1969). A summary of these results was given in Beltaos and Rajaratnam (1973), and review in the monograph of Rajaratnam (1976). The Russian investigations were based on mean velocity measurements using Pitot tube. The jet was observed to penetrate into the counter flow up to a penetration length and was then deflected backward.

Holly et al. (1972) published an article on the concentration study in an open channel to investigate the dilution of highly concentrated salt-water solution into another body of water. They used a conductivity meter to measure the concentration distribution. The Russian data were reanalyzed by Beltaos and Rajaratnam (1973), they also reported additional measurement data. An empirical expression was proposed for similarity velocity profile.

Morgan et al., 1976 reported a slightly different investigation, which was focused on the jet penetration in turbulent counter flowing pipe and the confinement effect of the enclosing pipe. With the recent advancement of laser-based flow diagnostic techniques (Hermann-Fottinger Institute of Fluid Mechanics, Technical University of Berlin, Germany) they revisited measurements on the mixing of a round jet in a counter flow. Accurate flow velocities were measured by LDA and concentration data were obtained from laser-induced fluorescence (LIF).

Lam and Chan (2002) studied the free counter flowing jet in an open channel setting. He got the mean concentration at different axial stations upstream of 0.7 the penetration

length and plotted them in the normalized form and compared them to the Gaussian distribution. They found that the concentration width of the jet is depending on the relative strength of the counter flow, and the counter flow enhances the spreading of the jet.

## CHAPTER 3


### Theoretical considerations

#### 3.1 Hydrodynamic study

The counter flowing wall jet, considering its expansion away from the jet opening could be approximately represented in an analytical form by a combination of a source and a uniform flow. Figure 3.1a shows a combination of uniform flow ( $U_M$ ) and a source of strength  $m$ , placed at the origin. The figure might be regarded as a plane of the flow adjacent to a side-contraction in a wide channel (flow past a half-body). Stagnation occurs at the point S, where the velocity is vanished. The dividing streamline can be regarded as a solid boundary and the velocity and pressure distributions along it can be determined analytically.

The considered  $\Psi$ -function is written as

$$\Psi = U r \sin\theta + m\theta, \quad (3.1.a)$$

  
 Uniform flow + Source flow

where

$$m = Q/2\pi, \quad (3.1.b)$$

Let  $Q$  and  $q_j$  denote the source flow and the jet discharge per unit width, respectively with

$$Q = q_j 2\pi/\alpha \quad (3.1.c)$$

and

$$m = q_j / \alpha, \alpha \text{ in radians.} \quad (3.1.d)$$

In two-dimensional case,

$$q_j = U_j h_j \quad (3.1.d)$$

Using Eq.(3.1.d) the expression for  $m$  becomes

$$m = q_j / \alpha = U_j h_j / \alpha \quad (3.1.e)$$

The position of the stagnation point S is given by

$$r_s = m / U_M \quad (3.1.f)$$

Replacing Eq. (3.1.e), the position of S becomes

$$r_s = U_j h_j / (\alpha U_M) \quad (3.1.g)$$

but the position of the stagnation point S can be expressed in terms of distances from the origin O as

$$r_s = x_s + d \quad (3.1.h)$$

Dividing by the jet opening  $h_j$ , the above equation becomes

$$r_s / h_j = (1 / \alpha) (U_j / U_M) \quad (3.1.i)$$

and

$$r_s / h_j = x_s / h_j + d / h_j \quad (3.1.j)$$

Therefore

$$d = h_j / \tan \alpha \quad (3.1.k)$$

The stagnation point S is at

$$x_s / h_j = (1 / \alpha) (U_j / U_M) - d / h_j \quad (3.1.m)$$

which represents the theoretical relationship of  $x_s$  versus the ratio between the velocities – the source velocity and the uniform velocity.

Using the expression for  $d$  in the stagnation point expression (Eq. 3.1.m)

$$x_s / h_j = (1 / \alpha) (U_j / U_M) - 1 / \tan \alpha. \quad (3.1.n)$$

When  $\alpha$  is very small,  $\tan \alpha \equiv \alpha$ , the equation becomes

$$x_s/h_j = (1/\alpha) (U_j / U_M) - 1/\alpha = (1/\alpha) (\lambda - 1) \quad (3.1.o)$$

where  $\lambda = U_j / U_M$  as a parameter.

Finally, the resulting equation is

$$x_s/h_j = (1/\alpha) (\lambda - 1) \quad (3.1)$$

Another way to demonstrate the same expression of the stagnation points is the following:

The stagnation point is at a distance  $r$  from the origin. Also, at this point, the uniform flow and source flow have equal velocities. Therefore, the discharge per unit width is

$$q = 2\pi r U = q_j 2\pi/\alpha \quad (3.1.1)$$

Further,

$$q_j = U_M r \alpha = U_j h_j \quad (3.1.2)$$

and

$$\lambda = U_j / U_M \quad (3.1.3)$$

The expression for the stagnation point becomes

$$r_s = \lambda h_j / \alpha \quad (3.1.4)$$

From Fig.3.1,

$$r_s = d + x_s \quad (3.1.5)$$

Finally,  $\alpha \approx \tan \alpha = h_j / d$  for  $\alpha \ll 5$  and

$$x_s = (\lambda - 1) h_j / \alpha \quad (3.1)$$

On the other hand, the equation for the  $\Psi$  line passing through the stagnation point S (Vallentine, 1967) is,

$$\Psi_S = U r \sin \theta + Q \theta / (2\pi) = Q/2 \quad (3.1.6)$$



This denotes the dividing streamline SRP (Fig. 3.1).

The streamline SRP for the counter jet is expected to follow the relation given in 3.1.6 only in the initial development zone of the return flow. As the main flow and the entrainment flow pass the jet exit section, DSL dips down. This is confirmed by the locus of the DSL traced on the basis of velocity surveys in the jet wake. This is discussed in Chapter 5 (Fig. 5.16).

### 3.2 Turbulent quantities

The mean flow is two dimensional, which means that,  $w = 0$ ,  $\partial / \partial z$  of any mean quantity is zero. Turbulent components

$$u'w' = 0, \quad v'w' = 0 \quad (3.2.1)$$

and since the mean flow is steady  $\partial u / \partial t = 0$  and  $\partial v / \partial t = 0$ .

The cross dimension of the flow is small. Therefore,  $u$  is much larger than  $v$  in a large portion of the jet, and velocity and stress gradients in the  $y$ -direction are much larger than those in the  $x$ -direction. With these considerations in mind, the equation of motion (continuity equation) could be reduced to the following form:

$$\partial u / \partial x + \partial v / \partial y = 0 \quad (3.2.2)$$

and the momentum equation

$$u \partial u / \partial x + v \partial v / \partial y = \nu \partial^2 u / \partial y^2 + (1/\rho) \partial \tau_t / \partial y$$

where  $\tau_t$  is the total shear stress (laminar and turbulent).

For the outer region

$$\partial u / \partial x + V \partial v / \partial y = \partial (-uv) / \partial y \quad (3.2.3)$$

the boundary conditions are

$$U \rightarrow 0 \text{ as } y \rightarrow \infty \quad (3.2.4)$$

The inner (or near wall) region equation becomes

$$0 = \partial (-uv) / \partial y + v \partial U / \partial y \quad (3.2.5)$$

where  $U = 0$  at  $y = 0$ .

Let us neglect the effect of any longitudinal-pressure gradient (Mathieu and Scott, 2000).

The behavior of the turbulent wall jets has been experimentally analyzed in detail by several authors. They remarked the absence of symmetry for the turbulent wall jets. The turbulent wall jet includes characteristics of the jet and the boundary layer. As a consequence, it possesses a dual turbulent structure representative of both free turbulence and wall layer turbulence. These two kinds of turbulence interfere everywhere but especially in the region where the velocity is a maximum. The shear stress is not zero at a point where the velocity is a maximum.

In a wall jet, one of the most significant quantities of the turbulent structure is certainly the shear stress  $-\rho u'v'$ , the distribution of which is not linked to the mean velocity gradient  $\partial U / \partial y$ . The role played by the mean velocity gradient on turbulent structures initially was analyzed in an isotropic state.

The energy balance equation was treated in different ways during a long period of time as a combination of the boundary layer and the free jet energy budget, but none of them give an understated explanation for a plane wall jets.

The equation of energy balance written by Hinze (1975) is the basic one, from which each of the researchers made their own assumptions and then plotted the turbulent energy equation details.

$$(u/2) \partial(k/2) / \partial x + (v/2) \partial(k/2) / \partial y + (u'^2 - v'^2) \partial u / \partial x + u'v' \partial u / \partial y$$

$$+ \partial \{v' [(k/2)/2 + p'/\rho]\} / \partial y + \varepsilon = 0 \quad (3.2.6)$$

Here,  $p$  is the pressure and  $\varepsilon$  the dissipation.

The turbulent kinetic energy is

$$k = \frac{1}{2} (u'^2 + v'^2 + w'^2) \quad (3.2.7)$$

Following Bradshaw (1961),  $k$  can be approximated by the expression

$$k = \frac{3}{4} (u'^2 + v'^2) \quad (3.2.7.1)$$

The kinetic energy balance model of the turbulent motion was adopted following Hanjalic and Launder (1972), which have been studied in a boundary layer case. The expressions for the individual components of the energy equation are the turbulence generation, convection, diffusion and dissipation terms

$$\text{generation: } -(u'v' \partial u / \partial y) \delta / U_m^3 \quad (3.2.8a)$$

$$\text{convection: } (u \partial k / \partial x + v \partial k / \partial y) \delta / U_m^3 \quad (3.2.8b)$$

$$\text{diffusion: } -[\partial (k v') / \partial y] \delta / U_m^3 \quad (3.2.8c)$$

$$\text{dissipation: } \varepsilon y_{0.5} / U_m^3 \quad (3.2.8d)$$

As known, the plane wall jet is the combination of the turbulent wall boundary layer and the free jet. A two-parameter model of turbulence for the last case was adopted from Rodi and Spalding papers (1983). The energy budget equation for turbulent free jet is

$$\begin{array}{ccccccc} U \partial k / \partial x + V \partial k / \partial y & = & \partial [(v_t \partial k / \partial y)] / \partial y & + & v_t (\partial U / \partial y)^2 & - & C_D k^{3/2} / L \\ \uparrow & & \uparrow & & \uparrow & & \uparrow \\ \text{convection} & & \text{diffusion} & & \text{shear} & & \text{dissipation} \end{array} \quad (3.2.9)$$

where  $v_t = -u'v' / (du/dy)$ ,  $C_D = 0.075$ ,  $L = -u'v' / [\sqrt{k} (du/dy)]$ , and for the same expression of  $k$  as the one from the turbulent wall boundary.

### 3.3 Mixing and dilution

The standard deviation was taken as the statistical measurement of concentrations for each sample set.

$$\sigma = \sqrt{\sigma^2} = \sqrt{\frac{\sum (C_i - C_{avs})^2}{N - 1}} \quad (3.3)$$

where  $\sigma$  is the standard deviation ,  $C_i$  is the sample concentration in terms of conductivity,  $C_{avs}$  is the average concentration of the section tested and  $N$  denotes the number of samples. The standard deviation is a measure of the distribution of the salt solution. Zero value of standard deviation  $\sigma$  denotes complete mixing. A larger value of  $\sigma$  denotes a very poorly mixed region.

## CHAPTER 4

### Experimental set-up and Procedure

#### 4.1 Experimental set-up and procedure for counter flowing wall jet studies

A flume 25.4 cm wide, 121.9 cm deep and 243.8 cm long was used to conduct the jet test (Figs. 4.1 and 4.1a). The counter flowing wall jet is introduced at the floor level of the flume. The jet openings are 2.54 cm, and 1.27 cm. These different jet openings were obtained by using appropriate streamlined Plexiglas inserts.

The incoming jet and the main flow pass through a set of screens and honeycombs to minimize the induced free stream turbulence in the flow. Proper turning vanes, screens, flow straightens and contracting sections preceded the wall jet nozzle to ensure a low level of background turbulence in the jet flow. The velocity measurements are made with the help of a two-dimensional Laser Doppler Anemometer system (Fig. A1). In the axial and vertical directions, the normal and shear stresses of the turbulence were measured besides the mean velocities. The combined flow of the main stream and the jet is measured by a standard 30° V-notch. The maximum error in the estimation of the discharge was 3%. As a check, the jet flow and the main flow are also independently measured by two independent venturimeters.

The test section has 0.5-inch thick plexiglas windows on the sides, top and floor of the test section. The two-dimensional laser probe is mounted on a three-axis automatic traversing mechanism that can be displaced in increments of 0.01- inch along each axis. The laser probe is mounted on a 3-D Velmex traverse. The probe can be moved in increments of 0.0025 mm along the x, y and z directions. The access to the jet centerline

through the test section floor ensures that the flow velocity in the axial direction and the lateral (span wise) directions can be measured very close to the boundary. The vertical component of the velocity can be approximately measured very close to the floor, if the two-dimensionality of the flow can be invoked. More details related to accuracy of modeling are provided in the Appendix.

#### **4.2 Equipment and methodology for dilution tests**

The test of the turbulent flow characteristics are supplemented by the studies related to the transport of TDS carried by the jet. To this end, surveys of the flow at selected locations in are conducted using a conductivity meter to determine the concentration distribution in jet wake. The purpose was to evaluate the counter flowing wall jet as a means to enhance the effective dilution of effluents in a stream.

A steel tank was used to inject salt solution into the pipe carrying the jet flow. The system has an air intake pipe placed at the top, a valve, a pressure regulator, a solution outlet, and a washing outlet for maintenance and cleaning at the bottom of the tank. The mixing characteristics of multiport diffuser would depend to a great extent on the geometric design and its orientation in the receiving water body. Figure 4.2 shows the sampling rake arrangement. Thirty-six copper tubes 1/8 inch in diameter and 6 inch long were used to get a good survey of the distribution of salt concentration over the half transversal flume section. The individual probes were connected with plastic tubing ( $\Phi 1/8''$ ) to reduce flow resistance and at the outlet with valves that permit a rigorous water sample collection.

Concentrations of samples are recorded using Conductivity Testr – OAKTON Instruments-TDS Tester 3<sup>TM</sup> that had a range of 0 to 1990  $\mu\text{S}$ .

## CHAPTER 5

### Analysis of the results

#### 5.1 Counter flowing wall jet characteristics

##### 5.1.1 Velocity distribution

The velocity distributions over the flow field of the test section have been surveyed using LDA techniques. Figures 5.1 and 5.2 provide typical velocity vector plots using the Stanford Graphics software. The velocity distribution (Fig. 5.1) is for the two-dimensional case of counter flowing wall jet with  $U_M = 0$  or  $\lambda = \infty$  (i.e. the plane wall jet). As pointed out by Launder and Rodi (1981), two-dimensionality of the flow is a key issue in studies of wall-jets (Abrahamsson et al., 1994). More over, as mentioned earlier, Fig. 5.2 shows the flow pattern of the entire flow field (test section) such as the jet flow expansion, the main flow, the recirculation zone, the expanding region of the combining flow behind the recirculation zone. The test data is given in Table 5.1 and 5.2 from the measurements made using LDA techniques at  $Re = 1.95 \times 10^4$  for  $\lambda = \infty$  and  $\lambda = 5.105$ , respectively.

Results related to wall jet obtained are compared with the results of other investigators in Fig. 5.3. The location of the jet where the velocity is 50% of the maximum jet velocity is denoted as  $y_{1/2}$ . For a length scale  $y_{1/2}$  and a velocity scale  $U_m$  defined earlier, the mean velocity profile is shown at  $x/h_j = 30$  at a  $Re = 2.57 \times 10^4$  ( $\lambda = \infty$ ) and the test data are listed in the table of Fig.5.3 (Table 5.3). There is a good agreement of the normalized mean velocity profiles up to  $y/y_{1/2} = 1.3$ . Wygnanski et al. (1992) show a Reynolds number dependence, and the LDA experiment of Karlsson et al. (1992) predicts

slightly lower velocities (Abrahamsson et al., 1994). These deviations are probably due to the influence of different measuring techniques that might cause certain deviations (Abrahamsson et al., 1994). For the case of counter flowing wall jet  $\lambda = 5.105$ , Fig. 5.4a provides simultaneous plot of the entire flow field with the velocity profiles measured at locations:  $x/h_j = 2, 10, 20, 40, 60, 74$ . One may observe a self-preservation of the mean velocity profiles up to  $x/h_j = 40$  (Fig. 5.4b) when the velocity and corresponding flow location are scaled with the local maximum velocity and half-width (i.e.  $y_{1/2}$ ).

### 5.1.2 Turbulent components

For the case of a wall jet flow, Fig. 5.5 shows the vertical distribution of turbulent shear stress obtained from the present data. For comparison some of the existing data are also included in Fig. 5.5. The slight variation in the trends of the shear stresses in Fig. 5.5 can be attributed to the variations in the Reynolds number and the axial (dimensionless) distance of measurement. A good agreement appears to be present. However, the normal stresses are contributing to the kinetic energy  $k$  for counter wall jet peaks faster ( $y/y_{1/2} = 0.6$ , Fig.5.6) than that for wall jets ( $y/y_{1/2} = 1.2$ , Fig.5.7). This information is useful for validation of results obtained from computational fluid dynamic (CFD) codes that generate turbulent characteristics of counter flowing jets.

Figure 5.8 provides a result of the turbulent energy balance for a profile at  $x/h_j = 30$ , using Eq. 3.2.9 with the convection term as closure.

The turbulent energy balance at  $x/h_j = 20$  and  $\lambda = 5.105$  it is given in Fig. 5.9. Note that the energy terms (Fig. 5.9) are normalized by the local value of  $U_m^2$  and the local value of  $y_{1/2}$ .



### 5.1.3 Jet expansion

For the wall jet flow, Fig. 5.10 shows the growth of the length scale  $y_{1/2}$  along the jet axis. There is a good agreement between the present data and the existing data. The jet expansion and the growth rate plots are linear and make an angle  $\alpha = 0.0686$  radians with the horizontal.

For the case of the counter flowing wall jet, Fig. 5.11 provides a plot of jet growth rate for different  $\lambda$  values covered in the present tests. This shows clearly an acceleration of growth rate as  $\lambda$  decreases and accordingly, the self-preservation zone of velocity profiles denoted by the linear segment appears to shrink and it gets reduced further until it vanished at lower  $\lambda$  values (Fig. 5.11). Data plots of jet growth rate shown in Fig. 5.11 also indicate that curves for different  $\lambda$  values take off from the linear growth rate of the wall jet ( $\lambda = \infty$ ) and bend more and more with decreasing  $\lambda$  value. Clearly, the jet expansion angle is nearly the same for both counter flowing jet and wall jet in the initial stage AB (Fig. 5.11). However, the jet expands much faster in the developing region BC (Fig. 5.11) and promotes a high degree of mixing in counter flowing jet.

### 5.1.4 Jet penetration

As defined earlier, the stagnation point S (Fig. 1.1b), denotes the section where the jet velocity is fully decayed. This permits the evaluation of the jet penetration distance,  $x_s$ .

The analytical expression (Eq. 3.1) derived in Chapter 3 for the jet penetration length  $x_s$  provides a good estimate when  $\alpha$  values resulting from the present test are used. For the fixed value of  $\alpha = 0.0686$ , Eq. 3.1 becomes

$$\frac{x_s}{h_j} = \frac{1}{0.0686}(\lambda - 1) \quad (5.1)$$

Thus,  $x_s$  was predicted for various tested  $\lambda$  values. Insert of Fig. 5.12 shows the results of other studies related to jet penetration. The agreement of the present data with existing data is reasonable.

### 5.1.5 Dividing Streamline and Recirculation Zone

For each set of velocity field survey data, the path of streamlines was traced to fix the geometry of the dividing streamlines (DSL) and that of the recirculation zone in the outer region of the jet expansion (Fig. 1.1b). Figure 5.13 shows a plot of the normalized geometry of the dividing streamline based on the data of present tests. One may observe in Fig. 5.13 that the maximum width of DSL occurs approximately at one third of  $x_s$  from the jet opening at a height

$$h = 0.575 x_s \quad (5.2)$$

The plotted plain curve PQR (Fig.5.13) is the predicted elliptic geometry of the DSL based on the results described in Chapter 3, simulated as part of the ellipse with half axis

$a = \frac{2}{3} x_s$ ,  $b = 0.575 x_s$  and centered at the  $x_s/3$ . The expression derived for this curve,

using the jet opening as the origin of coordinates is:

$$\frac{\left(x - \frac{1}{3}x_s\right)^2}{\left(\frac{2}{3}x_s\right)^2} + \frac{y^2}{(0.575x_s)^2} = 1 \quad (5.3)$$

Similarly, Fig. 5.15 includes the geometry of the recirculation zone. The variation of the dimensionless jet width  $h/h_j$  with  $\lambda^2$  is shown in Fig. 5.14.

## 5.2 Mixing and Dilution

Turbulent mixing characteristics of the counter flowing wall jet are studied experimentally. Here, the objective is limited to the determination of the effect of counter flowing wall jet on the mixing and propagation of injected dissolved solids (TDS) across the flow field in the wake behind the jet opening. Knowing the optimal distance of expected total mixing in the jet wake is of primer importance.

### 5.2.1 Survey of injected TDS concentration using conductivity meter

Various sets of water samples were obtained experimentally covering a region from  $30h_j$  to  $140h_j$  downstream of the jet opening and for range of flow setting with  $\lambda$  from 5 to 15. Here,  $h_j$  is the jet opening. For each flow setting, experimental data related to the concentration was collected while the velocity ratio  $\lambda$ , the main channel discharge  $Q_M$ , the jet discharge  $Q_j$  and the concentration  $C_j$  in the injected jet were varied. The combined discharge by weighted mass based on area of influence of the sampling point (Fig. A3) of all samples was recorded. One may note that the concentration of the main flow is hypothetically assumed as  $C_M = 0$ .

### 5.2.2 Total mixing

For each flow setting, denoting a fixed  $\lambda$ , fixed  $Q_M$ , fixed  $Q_j$  and fixed initial concentration of pollutant  $C_j$  (salt in water), samples were collected across several sections in the jet wake to determine the variation of salt concentration  $C$ . The procedure is shown in Figs. A3 and A4.

Figure A4 is a typical plot of dimensionless concentration standard deviation expressed as a function of axial distance  $x/x_s$  for the sub range  $\lambda = 8 - 11$ . Using such plots for various sub ranges of  $\lambda$  values covered in the tests (5 - 8, 8 - 11 and 11 - 15), the following equation is developed:

$$\frac{x}{x_s} = -0.112\lambda - 1.5 \quad (5.4)$$

The deviation of results from this relationship is within  $\pm 3\%$  following the arrangement of test data for various  $x$  and ranges of  $\lambda$  values covered (Fig.5.17).

### 5.2.3 Cross flow propagation of injected dissolved solids (salt)

Figure 5.16 shows a plot of a set of recorded sample concentrations derived from conductivity meter data. The outer envelope curve is selected as a conservative estimate of the concentration distribution of injected dissolved solid. For instance, the point  $C/C_{avs} = 0$  and  $C/C_{avs} = 1$  are the limiting values.

The location of the sampling profile provides the streamwise distance downstream of the jet opening. Test data of concentration survey is listed in Table 5.16. Clearly, the scatter of data is traced to the deviation of the flow from the assumed two-dimensional case. For the present test data set, all cross flow distances and axial distances are normalized by the jet penetration length  $x_s$ . Using these notations, one gets Eq.(5.5) and (5.6) for the limiting cases.

$$\text{For the limit of } C/C_{avs} = 0: \frac{y_0}{x_s} = 0.013\lambda^2 - 0.361\lambda + 2.904 \quad (5.5)$$

$$\text{and for limit of } C/C_{avs} = 1: \frac{y_1}{x_s} = 0.021\lambda^2 - 0.582\lambda + 4.901 \quad (5.6)$$

Here,  $y_{0,1}$  denotes the cross flow distance from the channel floor and  $x_s$  the corresponding jet penetration distance for the known  $\lambda$ . Figure 5.18 provides a plot of the above empirical relationships  $y/x_s$  versus  $\lambda$  (Eqs. 5.5 and 5.6). More over, the data have shown clearly that the propagation of injected matter is far beyond the limit of the DSL.

The jet penetration length  $x_s$  (Eq. 3.1) was found to be quite a reliable length scale for counter flowing wall jets.

## CHAPTER 6

### Summary and Conclusions

#### 6.1 Summary of results

The studies of some mean and turbulent characteristics of counter flowing wall jet and their application in Environmental Engineering have been carried out.

**6.1.1 Validation:** Validation of the present experimental procedures and equipment systems were made based on data collected from the LDA tests (counter wall jet flows,  $U_M = 0$ ). Wall jet test results indicate a good agreement with the existing data. These data include the mean velocity (Fig. 5.3), shear stress (Fig.5.5), kinetic energy (Fig. 5.5) and wall jet expansion  $\alpha$  (Fig.5.10) for wall jets.

The overall results and contributions of the present study can be summarized in terms of the following conclusions:

1. A hydrodynamic model can be developed to predict the counter jet penetration length  $x_s$ . For the range  $3 < \lambda < 6$ , test data agreed with the predicted value of  $x_s$ .
2. The jet expansion angle  $\alpha$  is nearly the same for wall jets and counter wall jets in the initial jet development zone AB (Fig. 5.11). However, downstream of this zone, the jet expands much faster in the main developing region BC. This promotes a high degree of mixing in the case of counter flowing wall jets.
3. The hydrodynamic model indicates that the developing region of the dividing streamline has the shape of an ellipse. The relationships proposed

(Eqs. 5.2 and 5.3) in the model for its geometry are verified by the shape of the experimental dividing streamline (DSL). The geometry of the recirculation zone was computed and traced on the basis of the velocity field survey data (Fig. 5.15).

4. The expected total mixing distance in the jet wake and the propagation of the injected total dissolved solids (TDS) can be predicted using empirical data (Eqs. 5.4, 5.5 and 5.6). Figures 5.17 and 5.18 provide the charts for design.
5. The jet penetration distance  $x_s$  and the mean velocity at the so-called half width ( $y_{1/2}$ ) serve as the proper scales to the counter jet flow.  $x_s$  itself is a function of  $y_{1/2}$ .
6. The reported data bank related to turbulence quantities will be useful for validation of CFD codes that generate such data.

## 6.2 Suggestions for future studies

The following are suggested for further studies:

1. The additional tests data for an extended range of settings ( $Re$ ,  $\lambda$ ) has to be obtained to provide a complete design chart data bank.
2. Computational Fluid Dynamics (CFD) codes could be built to cover a wider range of flow setting parameters and conditions and also to validate the present data.
3. Mixing characteristics of a counter flowing wall jet in the developing region of jet opening may be studied to find out the behavior of the jet.

4. The inclined counter flowing wall jet may provide more light on the effect of jet orientation on mixing and dilution.
5. The region of study AB in the jet wake ought to be extended to a longer reach to reduce errors due to extrapolation (Fig. A4).



## References

1. Abrahamsson, H., Johansson, B. and Löfdahl, L. (1994) "A turbulent plane two-dimensional wall-jet in a quiescent surrounding" *European Journal of Mechanics, B/Fluids*, 13, n° 5, 533-556
2. Balachandar, R., Robillard, L. and A.S. Ramamurthy (1992) "Some characteristics of counter flowing wall jets" *Transactions of the ASME*, vol. 114, 554-558
3. Bradbury, L.J.S (1965) "The structure of a self-preserving turbulent plane jet" *J. Fluid Mech.*, vol. 23, 31-64
4. Bradshaw, P. (1967) The turbulent structure of equilibrium Boundary layers, *J. Fluid Mech.*, Vol. 29, pp. 625-645
5. Bradshaw, P. (1971) *An introduction to turbulence and its measurement*, Pergamon Press Ltd.
6. Bradshaw, P. and Gee, M.T. (1962) "Turbulent wall jets with and without an external stream" *Aeronautical Research Council Reports and Memoranda*, London, No. 3252
7. Bradshaw, P. (1994) "Turbulence: the chief outstanding difficulty of our subject" *Experiments in fluids* 16, 203-216
8. Buchhave, P. and William K. George, Jr., J.L. Lumley (1979) "The measurement of turbulence with the Laser-Doppler Anemometer" *Ann. Rev. Fluid Mech.*, 11, 443-503
9. Daily, J.W., and Harlemann, D.R.F. (1966) "Fluid Dynamics"

10. Eriksson, J.G., Karlsson, R.I. and Persson, J. (1998) "An experimental study of two-dimensional plane turbulent wall jet" *Experiments in Fluids*, Springer-Verlag, 25, 50-60
11. Fujisawa, N. and Shirai, H. (1987) "Measurement of turbulence energy balance in a two-dimensional wall jet along a plane surface", *Nippon Kikai Gakkai Ronbunshu*, 53, No. 491, 1947-1952
12. George, W., Abrahamsson, H., Eriksson, J. and Karlsson, R.I. (2000) "A similarity theory for the turbulent plane wall jet without external stream" Cambridge University Press, *J. Fluid Mech.*, vol. 425, 367-411
13. Gerodimos, G., So R.M.C. (1997) "Near-wall modeling of plane turbulent wall jets" *J.Fluid Eng.*, 119, 304-313
14. Glauert, M.B. (1956) "The wall jet" *J. Fluid Mech.*, 1, 625-643
15. Hanjalic, K. and Launder, B.E. (1972) "A Reynolds stress model of turbulence and its application to thin shear flows" *J. Fluid Mech.*, vol. 52, part 4, 609-638
16. Heskestad, G. (1965) "Hot -wire measurements in a plane turbulent jet" *J. of App. Mech.*, 721-734
17. Hinze, J. O. (1975) "Turbulence" 2<sup>nd</sup> Ed., McGraw-Hill, USA
18. Hopkins, D.F. and J.M. Robertson (1967) "Two-dimensional incompressible fluid jet penetration" *J. Fluid Mech.*, vol. 29, part 2, 273-287
19. Hsiao, F.B. and Sheu, S.S. (1994) "Double row vortical structures in the near field region of a plane wall jet" *Experiments in Fluids*, 17, 291-301

20. Johansson, G.T. and Karlsson, R.I. (1989) "The energy budget in the near-wall region of a turbulent boundary layer" *Applications of Laser Anemometry to Fluid Mechanics*
21. Lam, K.M and Chan, C.H.C. (2002) " Time-Averaged Mixing Behavior of Circular Jet in Counterflow: Velocity and Concentration Measurements" *Journal of Hydraulics Engineering*, Vol. 128, No. 9, 861-865, September 1, 2002.
22. Laufer, B.E and Rodi, W. (1981) "The turbulent wall jet" *Pergamon Press*, vol. 19, 81-128
23. Ljuboja, M. and Rodi, W (1980) "Calculation of turbulent wall jets with an algebraic Reynolds stress model" *A.S.M.E, J. Fluid Eng.*, vol. 102, 350-356
24. Laufer, B.E. and Rodi, W. (1983) "The turbulent wall jet-Measurements and Modeling" *Ann. Rev. Fluid Mech.*, 15, 429-459
25. Laufer, J. (1950) "Investigation of turbulent flow in two-dimensional channel" *Report 1053, NACA, TN 2123*
26. Mathieu, J. and Scott, J. (2000) "An introduction to turbulent flow" *Cambridge University Press, UK*
27. Moawad, A.K., (1998) "An experimental study of dilution and mixing with turbulent jets in cross flows", *PhD thesis*,
28. Peavy, H.S., (1985) *Environmental engineering*, McGraw-Hill, Inc.
29. Qasim, S.R. (1999) *Wastewater treatment plants*, Technomic Publishing Co.
30. Rajaratnam, N. (1976) "Turbulent Jets" *Elsevier, Developments in Water Science*, 5, The Netherlands

31. Ramamurthy, A.S., Diep Vo and Tudor Magdalena, (2002) "Characteristics of counter flowing wall jets" Annual Conference of the Canadian Society for Civil Engineering, June 5-8, Montreal, Quebec, Canada
32. Robillard, L., A.S. Ramamurthy (1974) "Experimental investigation of the vortex street generated by a plane jet in a counter flow" Transactions ASME, 43-48
33. Rodi, W. and Spalding, D.B. (1983) "A two-parameter model of turbulence, and its application to free jets" London, paper 2, 22-32
34. Saghravani, S.F., (2002) "Turbulence characteristics of counter flowing free jets" PhD thesis, Concordia University, Montreal, Canada
35. Schlichting, H. and Gersten, K. (2000) "Boundary Layer Theory" Mayes K, Trans., Springer, Germany
36. Schneider, M. E., (1987) "Laser Doppler measurements of turbulence in a two-dimensional wall jet on a flat plate in stagnant surroundings" PhD thesis, University of Minnesota
37. Tailland, A. et J. Mathieu (1967) "Jet parietal" Journal de Mécanique, vol.6, No. 1, mars, 103-131
38. Tangemann, R. and Gretler, W. (2001) "The computation of a two-dimensional turbulent wall jet in an external stream" Transactions of ASME, J. Fluid Eng., vol. 123, 154-157
39. Vallentine H. R. (1967) Applied Hydrodynamics, New York Plenum Press
40. Wilcox, D. C. (1993) "Turbulence modeling for CFD" DCW Industries Inc
41. Wygnanski, I. and Fielder, H. (1969) "Some measurements in the self-preserving jet" J. Fluid Mech., 38, 577-612

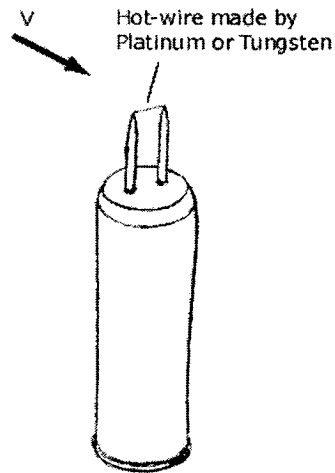
## Appendix

### I. Equipment for Flow Measurements

An anemometer is an instrument for measuring fluid velocity. Whether there are gases or fluids, hot wire or hot film, anemometers measure fluid speed using a delicate probe made of thin tungsten/platinum wire, or a thin metallic film. This probe is heated to a temperature higher than average temperature of the fluid. Using sophisticated circuitry, the anemometer stabilizes and maintains the probe temperature at a constant level throughout the measurement. Since the fluid flowing past the probe has a lower temperature than the probe, the film/wire is constantly being cooled by the fluid flow. Therefore, the higher the velocity is it, the faster the rate of cooling. Since the anemometer must maintain the probe temperature at a constant level, it is therefore sensitive to the rate at which it is being cooled, i.e., the fluid velocity. This velocity is translated to a continuously changing voltage, which has a nonlinear relationship with the flowing fluid. This voltage then undergoes signal conditioning, to filter out noise and improve the Signal/Noise ratio. After proper calibration of the probe channels, it is possible to measure fluid velocities with an accuracy of 0.05% or greater, depending upon the measurement range and the quality of the calibration. The response time between measurement and instrument output is very short in comparison with other methods of fluid flow measurement and can reach a minimum of 1/2 microsecond ([www.efunda.com](http://www.efunda.com)).

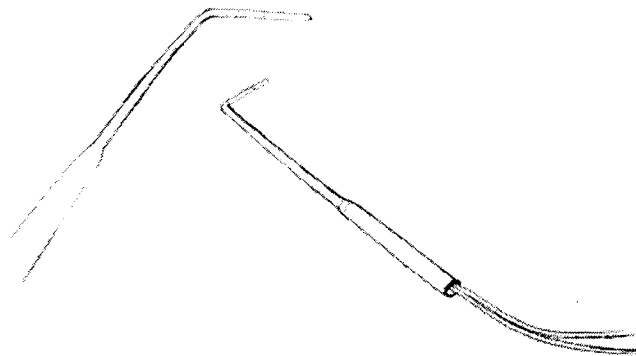
The Hot-Wire Anemometer is the most well known thermal anemometer, and measures a fluid velocity by noting the heat convected away by the fluid. The core of the anemometer is an exposed hot wire either heated up by a constant current or maintained

at a constant temperature (refer to the schematic below). In either case, the heat lost to fluid convection is a function of the fluid velocity.



Typical Hot-Wire Anemometer

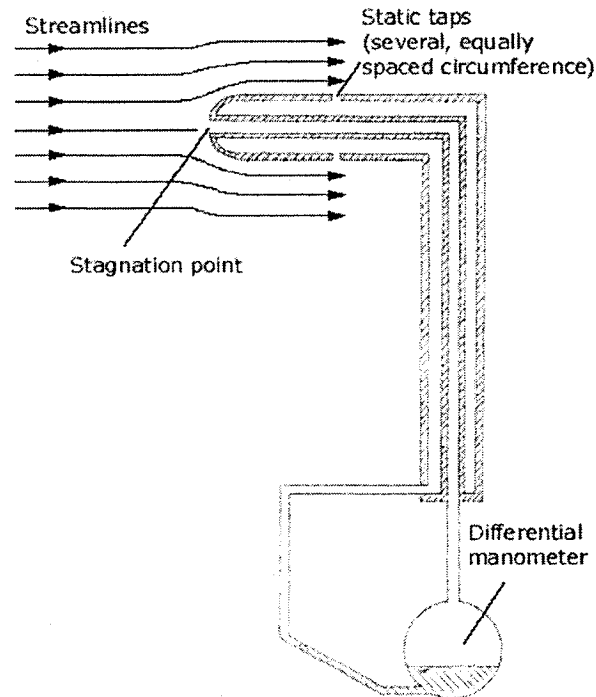
A Pitot-static tube is a flow velocity meter, which is capable of measuring fluid velocities as a localized point (as opposed to an averaged velocity across a larger section). A schematic of a Pitot tube is shown below.



Typical Pitot Static Tube

The Pitot tube yields a pressure measurement, which is typically measured with a differential manometer. The Pitot tube (named after Henri Pitot in 1732) measures a fluid velocity by converting the kinetic energy of the flow into potential energy. The

conversion takes place at the stagnation point, located at the Pitot tube entrance (see the schematic below). A pressure higher than the free-stream (i.e. dynamic) pressure results from the kinematic to potential conversion. This "static" pressure is measured by comparing it to the flow's dynamic pressure with a differential manometer.



Cross-section of a Typical Pitot Static Tube

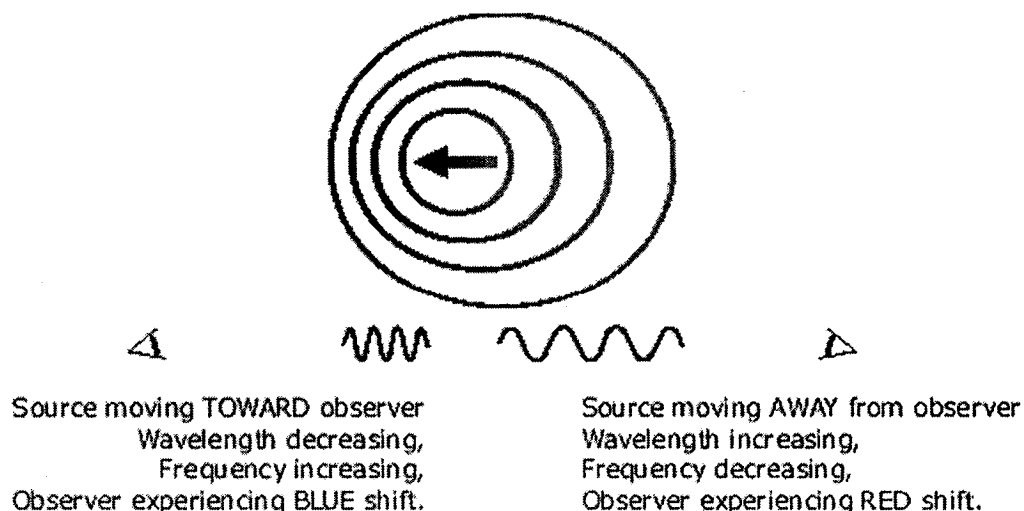
Converting the resulting differential pressure measurement into a fluid velocity depends on the particular fluid flow regime the Pitot tube is measuring. Pros: Simple construction; Relatively inexpensive; Almost no calibration required; Induces minimal pressure drops in the flow; Requires only a few access holes into the flow conduit; no wide-open cut needed. Cons: Accuracy and spatial resolution may not be high enough for some applications; Tube must be aligned with the flow velocity to obtain good results.

## II. Measurement of turbulence with the Laser-Doppler Anemometer

The laser velocimetry technique is a non-invasive flow measurement technique. Laser velocimetry is used for measuring flow velocities in combustion mixing, flames, rotating machinery, narrow channels, chemically reacting flow, wave tanks, wind or water tunnels, and in other various applications where conventional techniques perform poorly.

Advantages of laser velocimetry are: measures flow reversals; no flow calibration required; no probe in the flow; senses only the velocity, independent of temperature, density and composition changes in the fluid, and finally precise measurements of velocity components.

The Doppler effect was named after Austrian physicist J. C. Doppler. He was the first who has been described it for sound in 1842. It states that waves emitted from a source moving toward an observer are squeezed, i.e. the wave's wavelength is decreased and frequency is increased, as shown in the schematic below. Conversely, waves emitted from a source moving away from an observer are stretched; i.e. the wave's wavelength is increased and frequency is decreased. The waves can be acoustic waves or electromagnetic radiation.





Turbulent flow characteristics were determined by a Dantec Laser-Doppler Anemometer (LDA) method. Dantec distributor has provided the measurement equipment and the software called Particle Dynamics Analyzer (PDA) System.

The LDA is an instrument for research on fluid flows that has the potential of allowing local time-resolved measurements of fluid velocity without disturbing the fluid phenomenon under investigation (no probe in the flow). The method is based on the measurement of the Doppler shift of laser light scattered from small particles carried along with the fluid.

The LDA system includes a laser, optics, photo detectors, and signal processor. The function of the optical system is partly to direct and focus the incident beams to a small volume within the flow field, and partly to collect the scattered light from this volume while simultaneously discriminating against ambient light and light scattered regions outside the volume (Fig. A1) (Buchave, 1979).

A region defined by the intersection of the two incident beams designates the probe volume, and the region in space from which Doppler signals are detected it designates the measuring volume. The measuring volume is more difficult to define than the probe volume. With the Gaussian laser beams the probe volume is an ellipsoid, and the probe volume dimensions are defined in terms of the half-axes of the ellipsoid in the coordinate system defined in Fig. A1.

The signal processor is a model Dantec 58N10, which it is a burst processor. Essentially it measures the time for a particle traversal through the measuring volume or through some finite length within the measuring volume. The processor operates on the

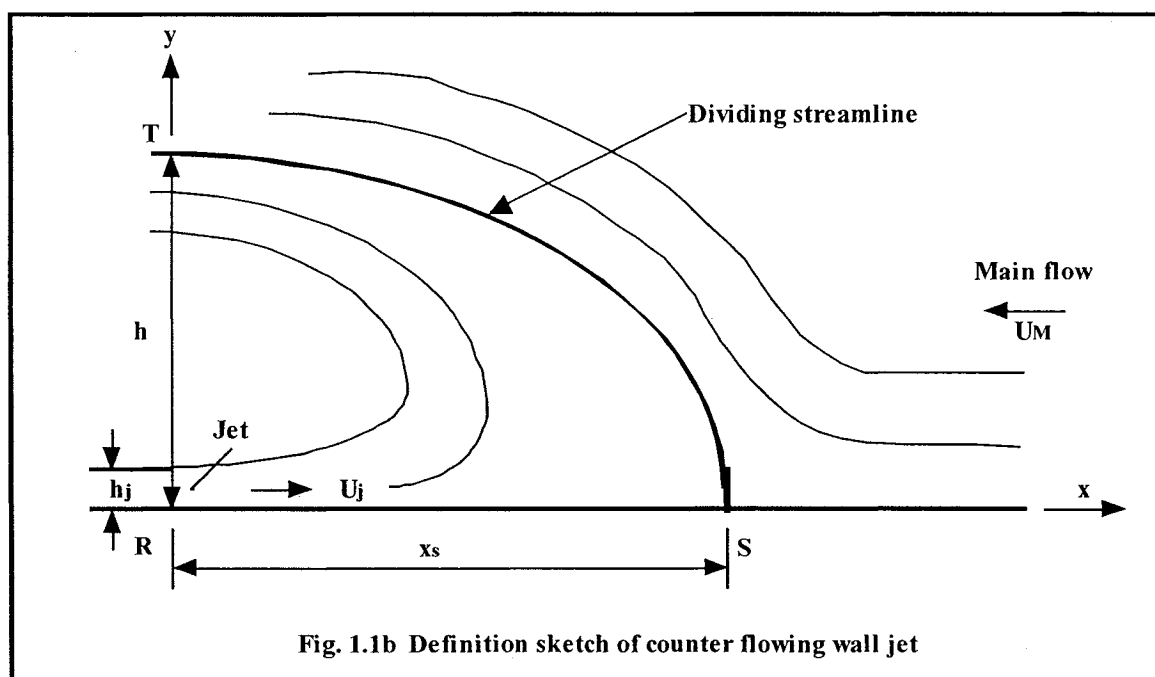
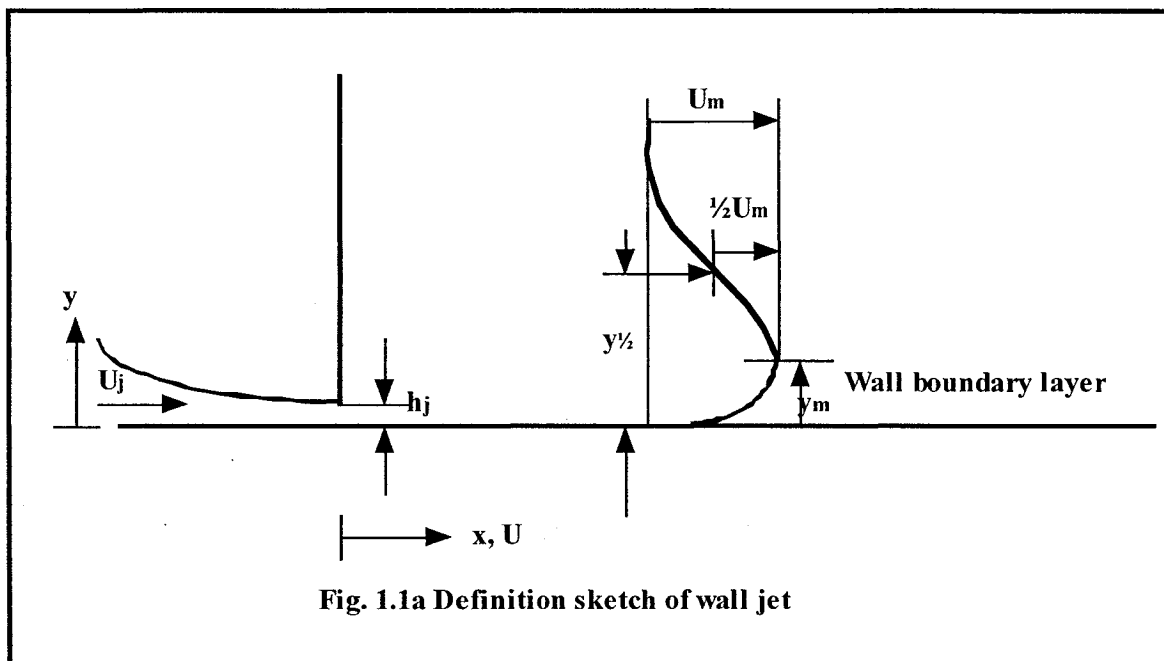
burst mode, which it is depending on the choice of parameters such as signal level and bandwidth.

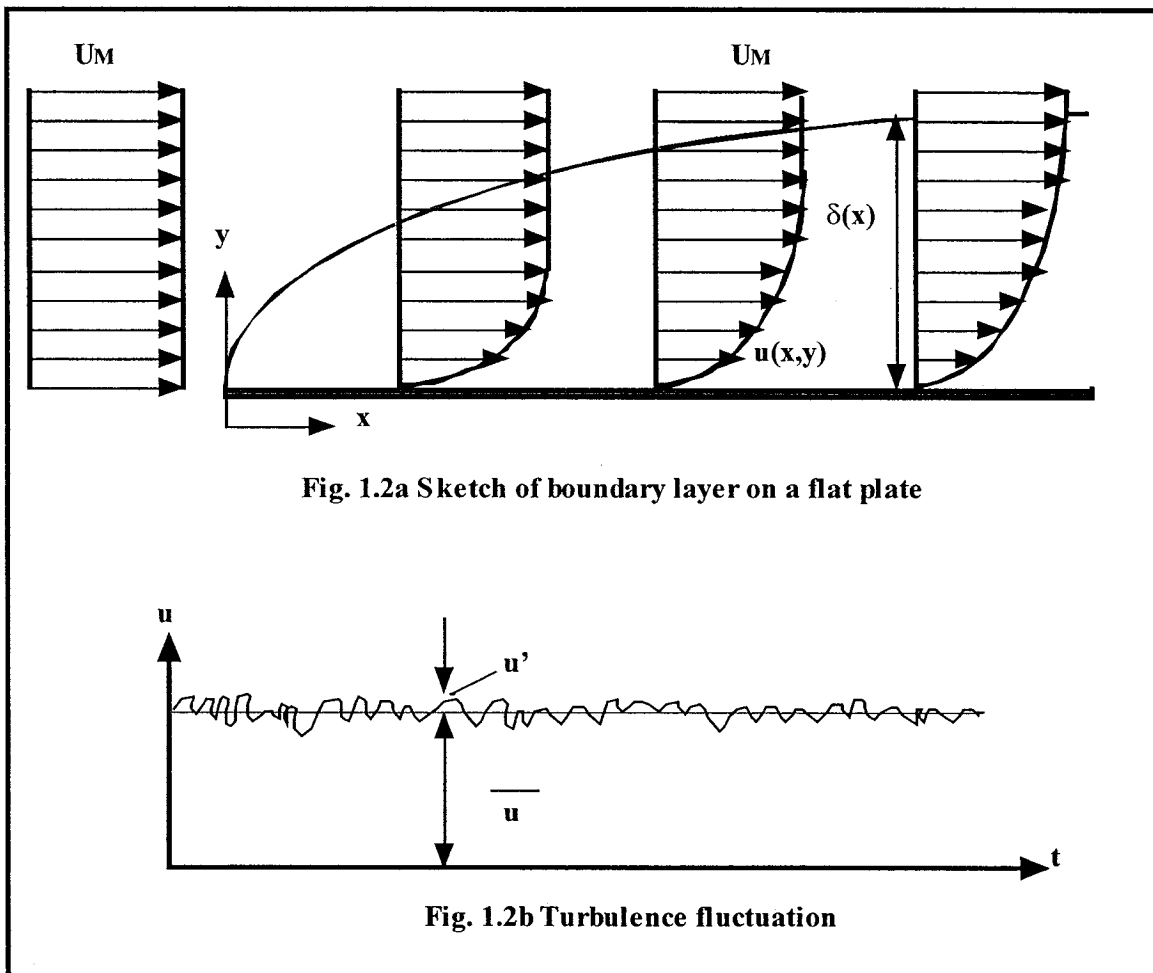
The laser is an Argon-Ion laser beam with two components fringe pattern. There are two pairs of beams with different wavelengths: the blue beam and the green beam. The laser beams have 1 mm diameter and there are situated at 38 mm apart. The relation between the Doppler frequency and the velocity  $u$  is linear, thus calibration is limited to the determination of the coefficient of proportionality given by the laser wavelength  $\lambda$  and the beam intersection angle  $\theta$ . Complete characterization of the turbulent velocity field requires simultaneous determination of all three velocity components.

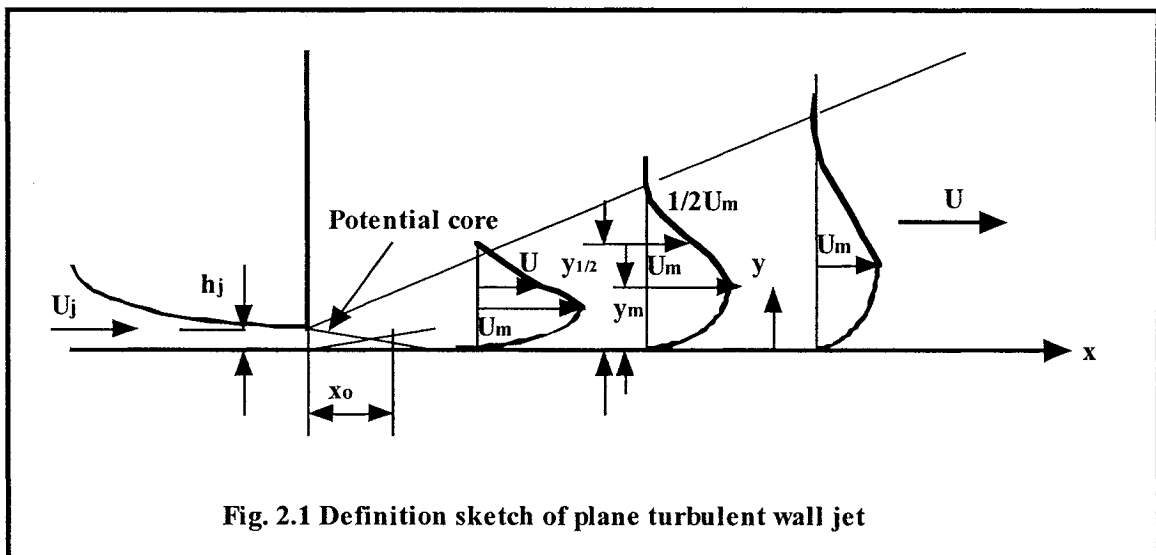
The properties of the Doppler signal and thus the proper method of signal processing depend on the number of particles present in the measuring volume, and the mode of operation of the detector optics. The LDA respond to the component of fluid velocity normal to the interference fringe planes in the probe volume. It is assumed that the particles follow the fluid motion exactly. The fluid has to be of constant density, and refractive index. The flow could be assumed incompressible, and the particles were statistically uniformly distributed throughout space.

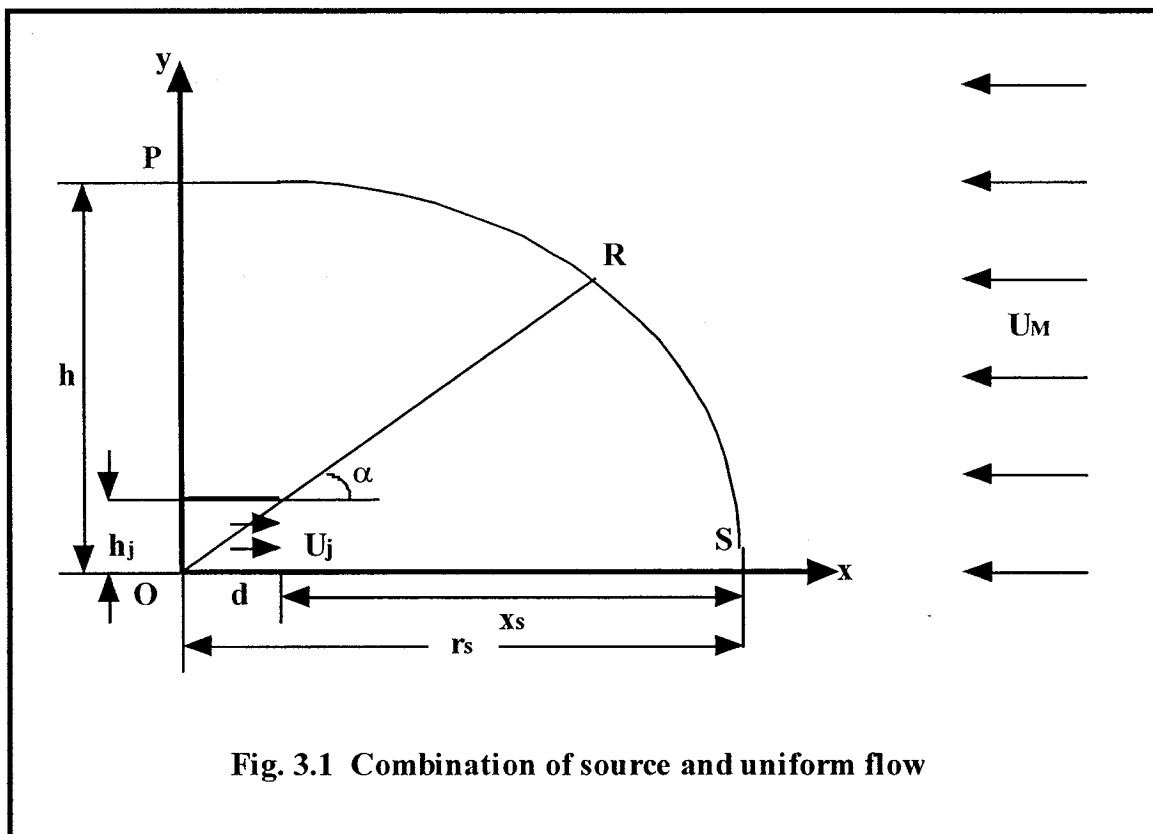
The main problem in burst detection LDA signal processing is the extraction of statistical quantities from the randomly sampled data accumulated by the processor. The best optical configuration is the dual beam, and the fringe-mode system. For the burst processor we can write the velocity signal directly since there are assumed to be only single particles present. If the burst signal is analyzed for the period of time the particle is in the volume (Fig. A2). The figure reproduces the instantaneous velocity of the scattering particle only while it is in the scattering volume.

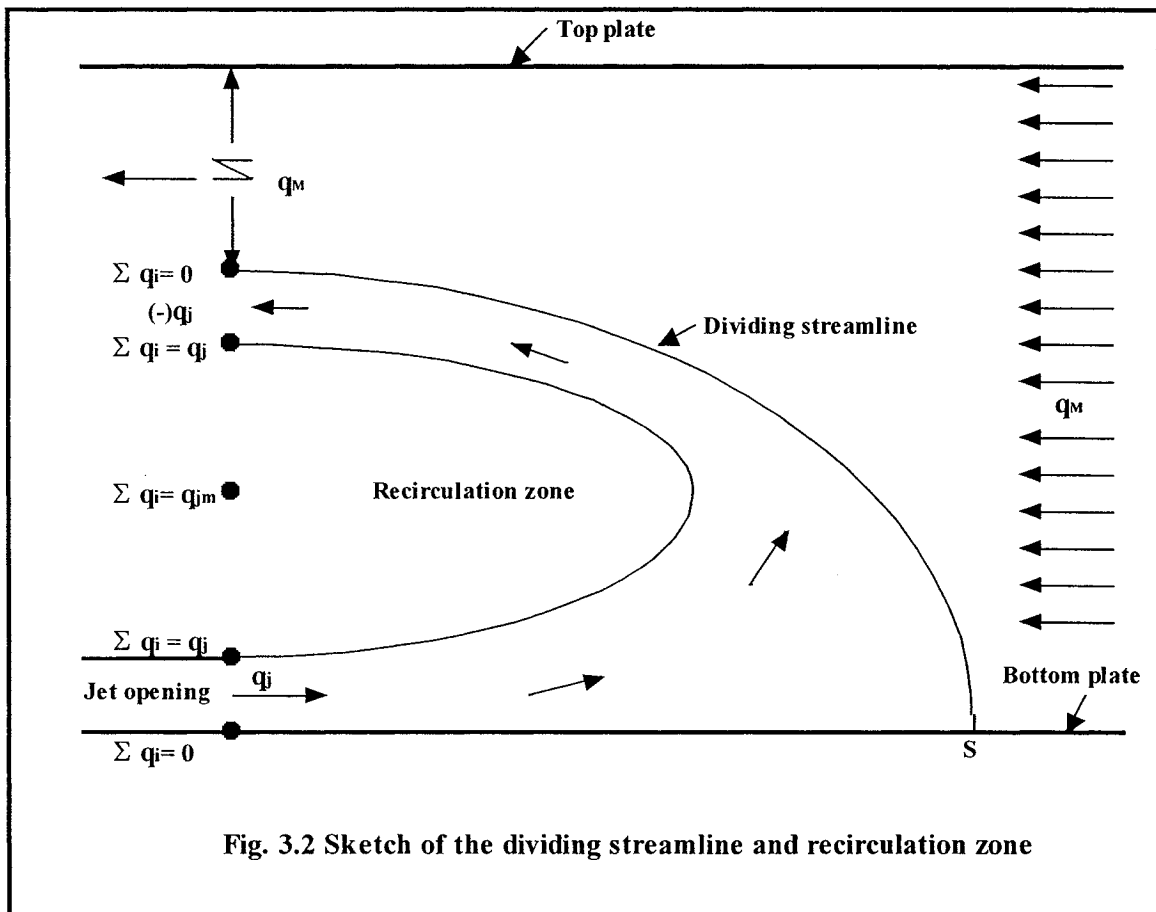
Most real processors measure the velocity during the burst; thus the velocity must be approximately constant during its traversal of the volume. The direction of the particle and its velocity are irrelevant; only the x-component and the transit time (successfully applied to measurements of mean velocity in a jet) matter.













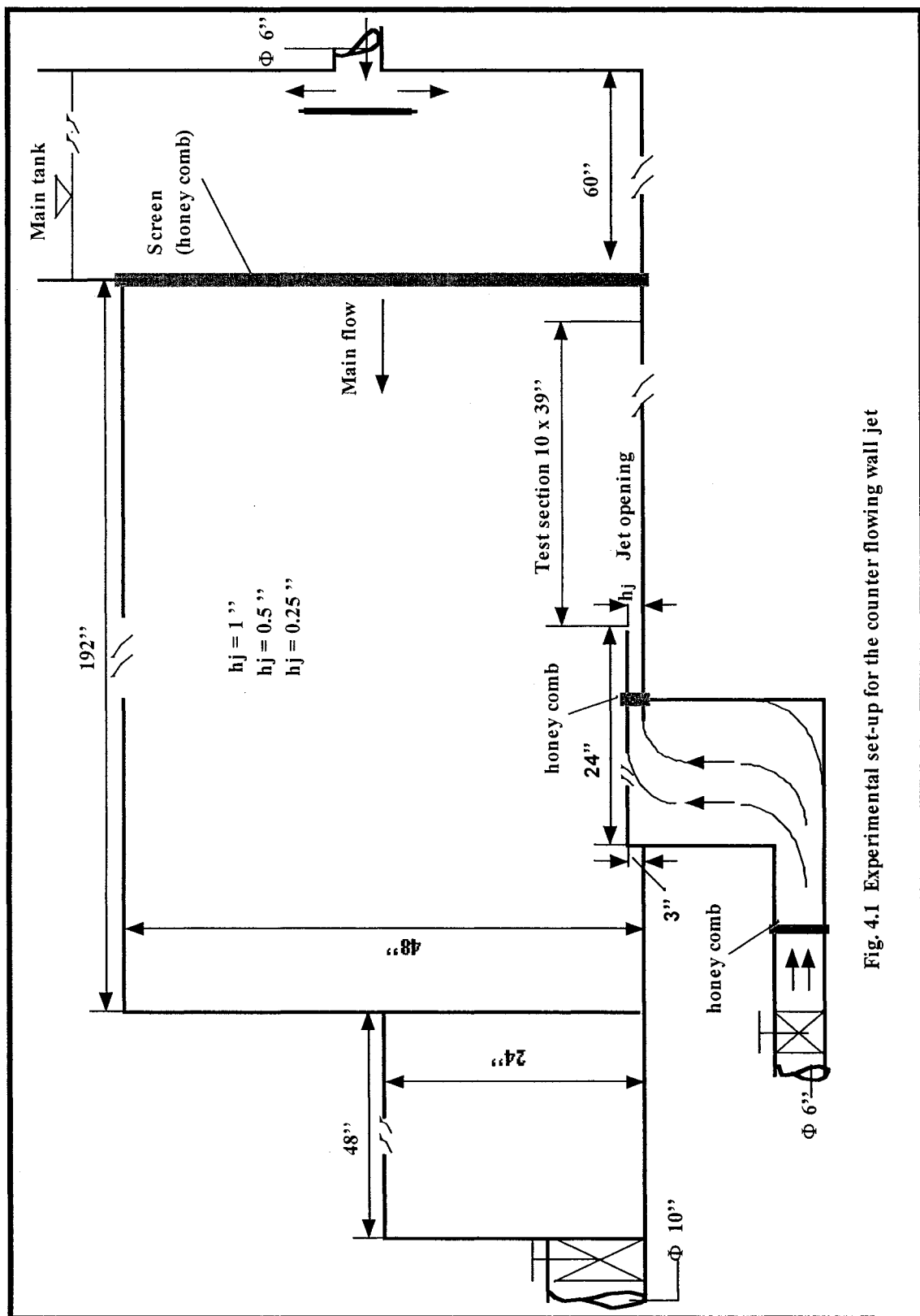
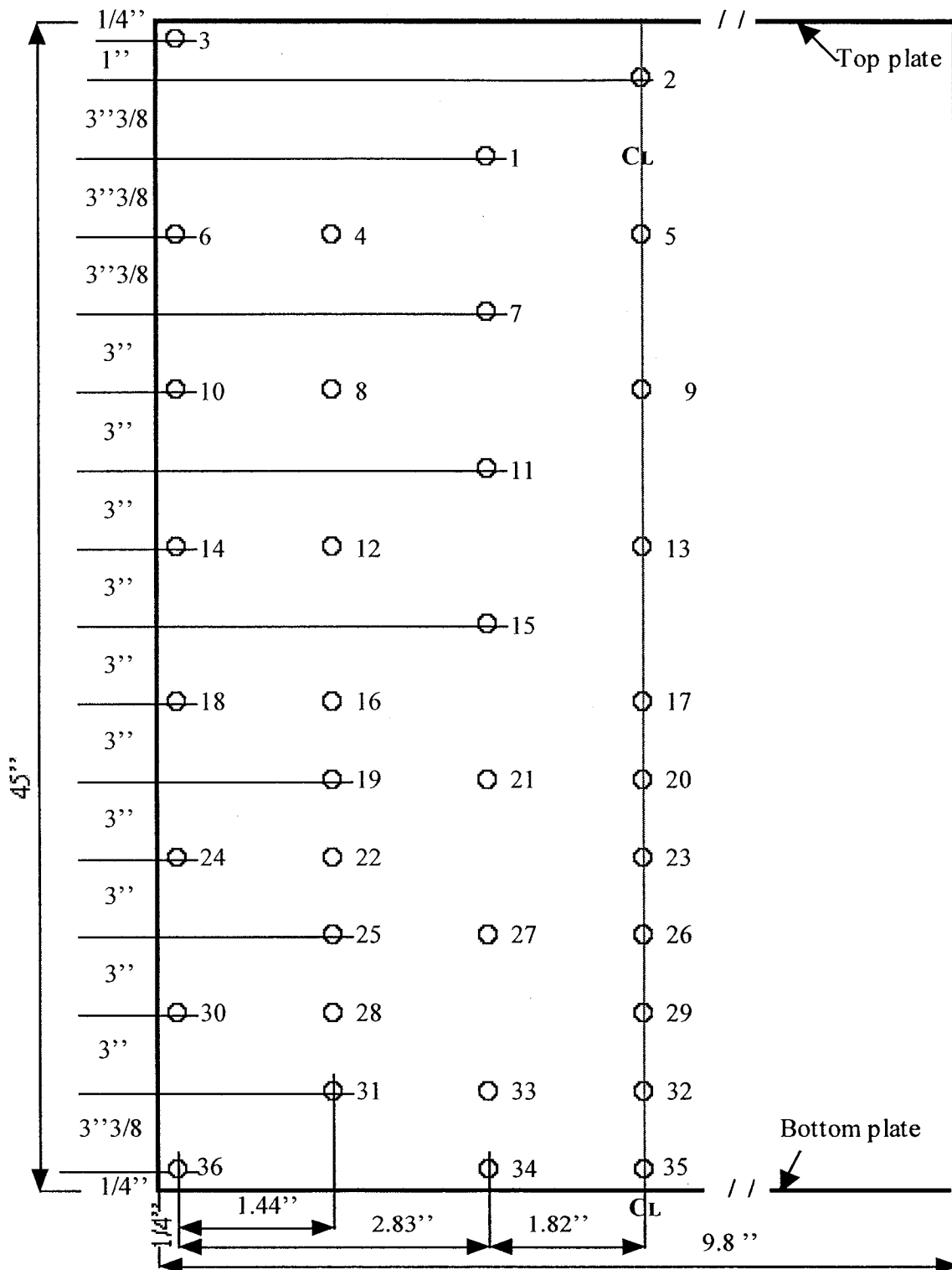


Fig. 4.1 Experimental set-up for the counter flowing wall jet



**Fig. 4.1a Traverse monitor (left side) and PDA monitor (right side) in front of test section**



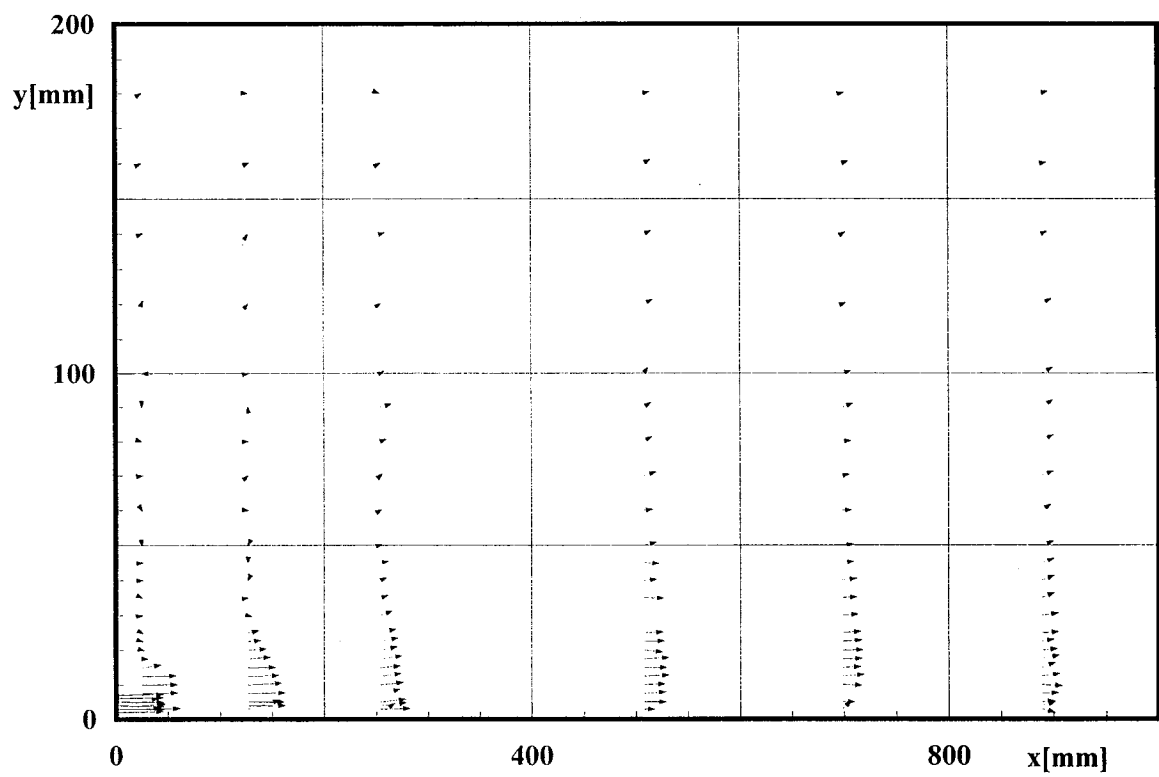
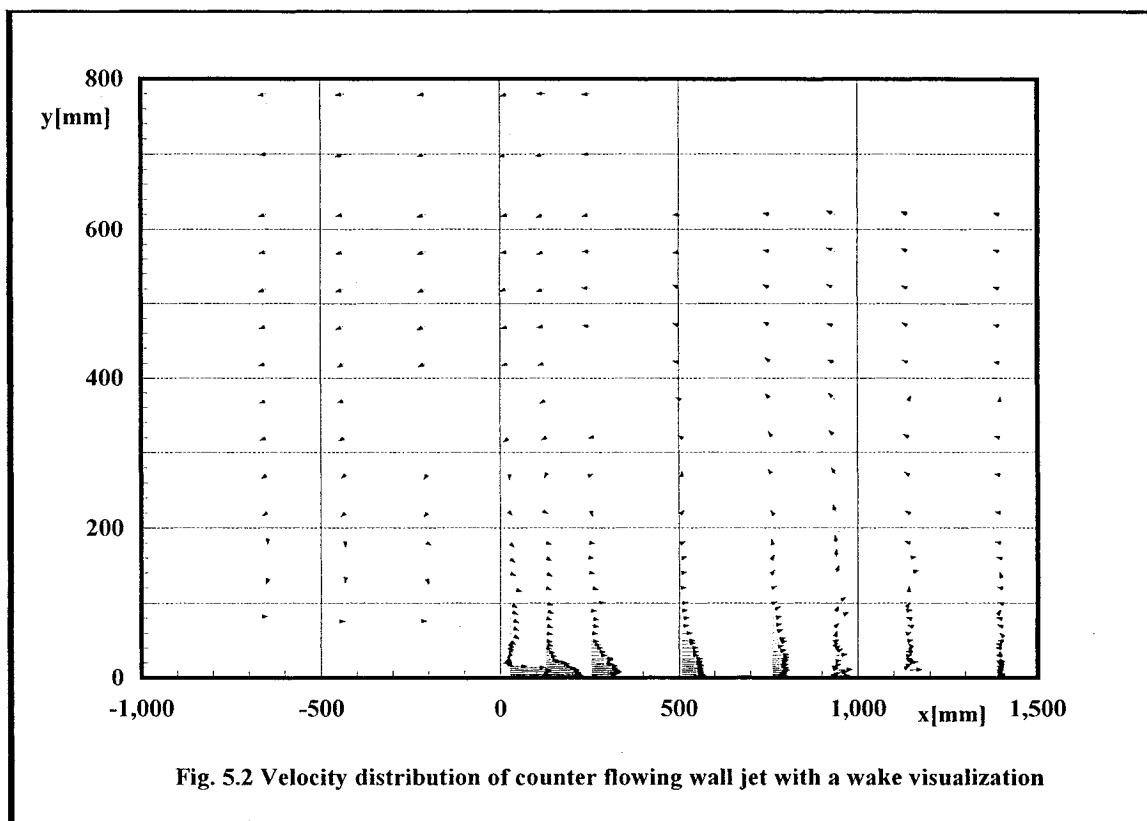
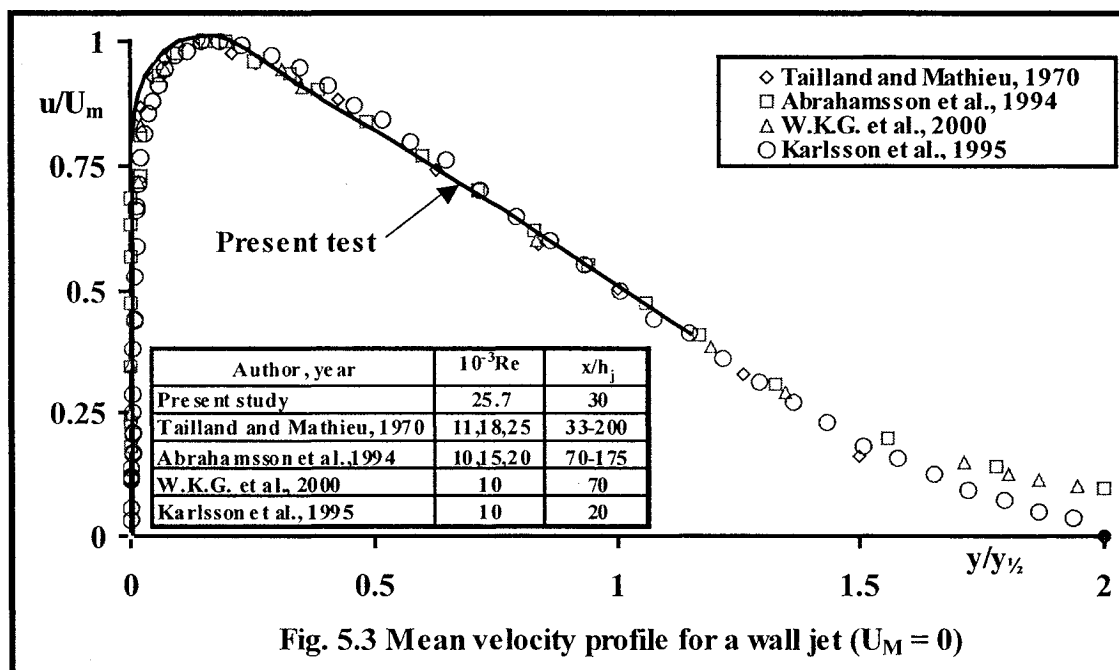
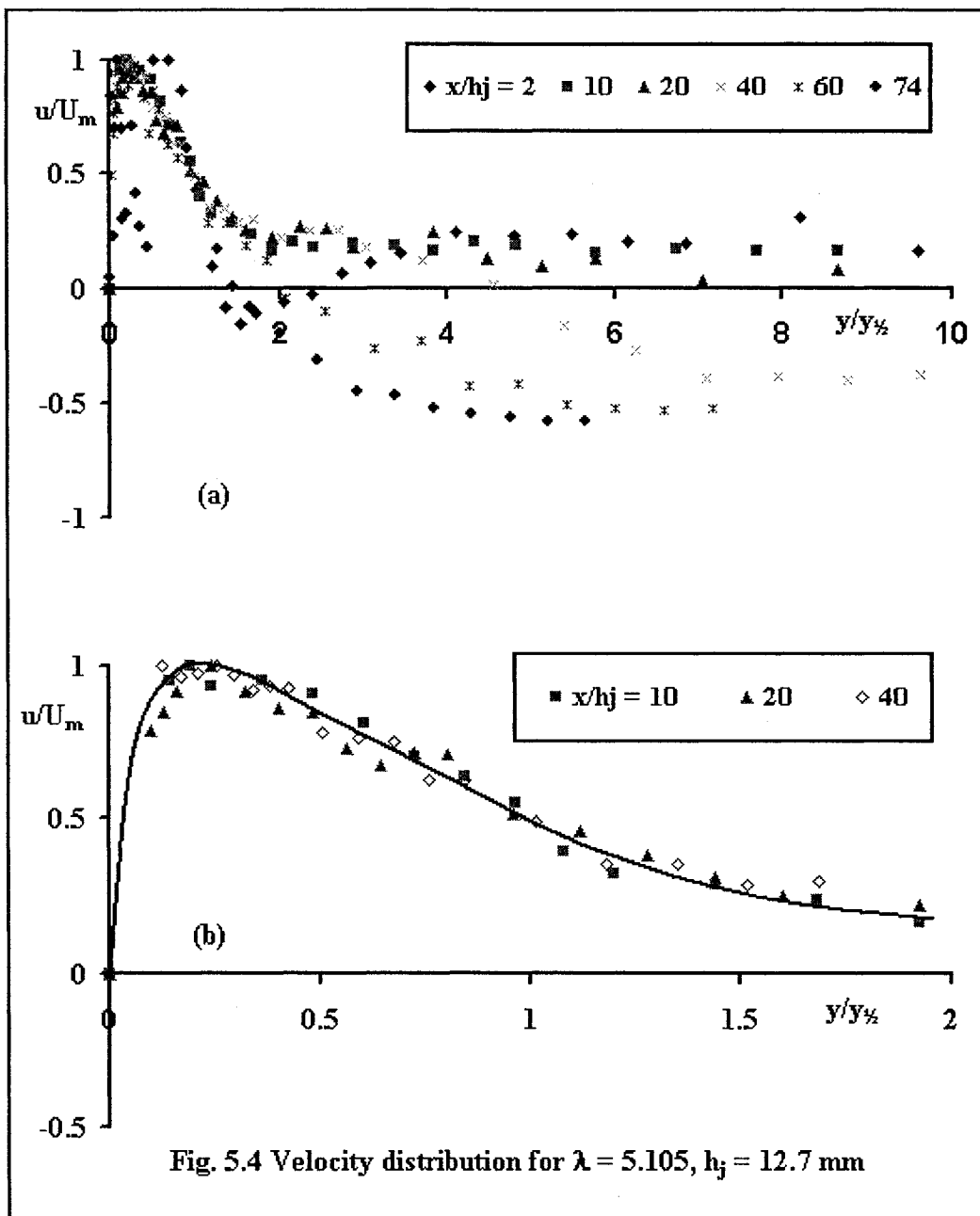
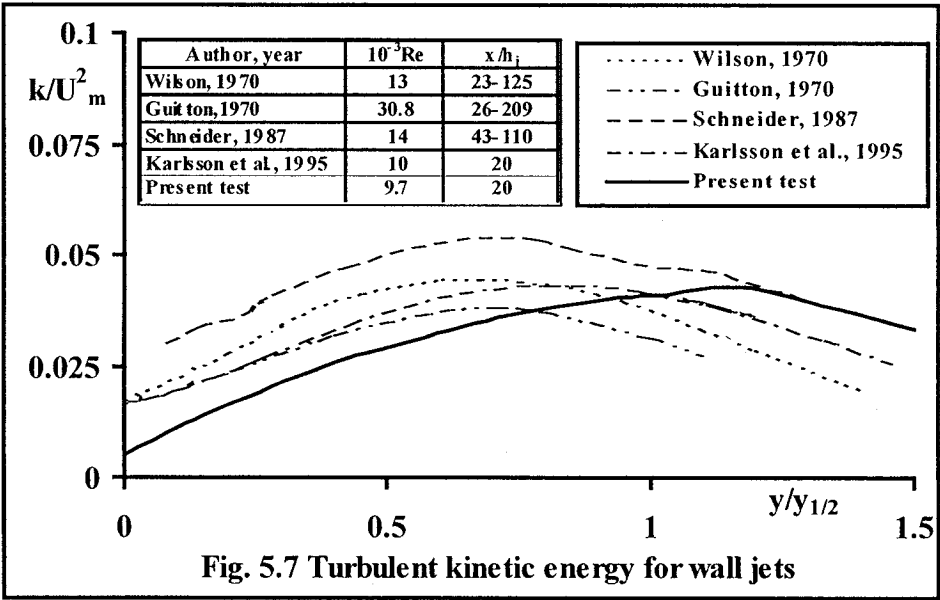
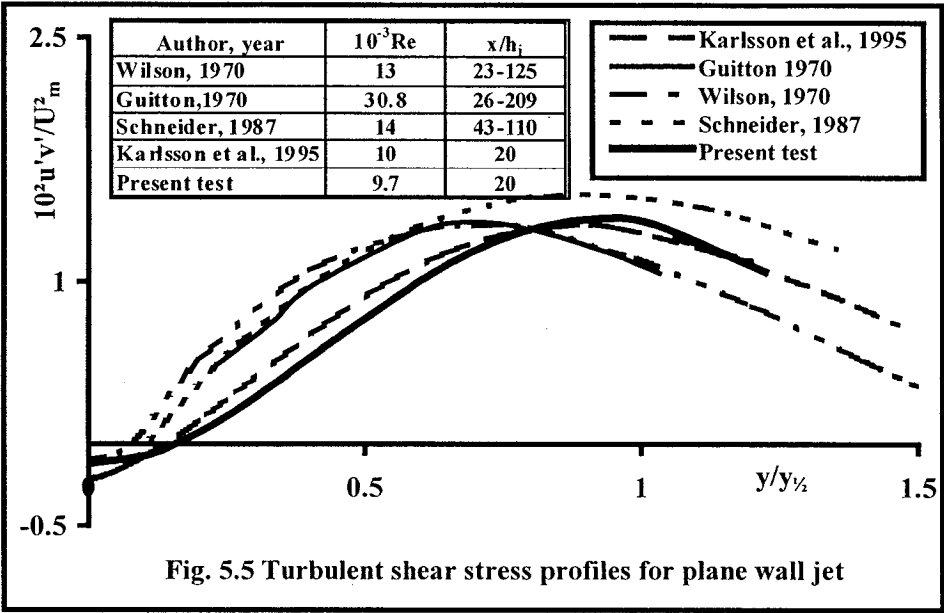


Fig. 5.1 Velocity distribution of plane wall jet

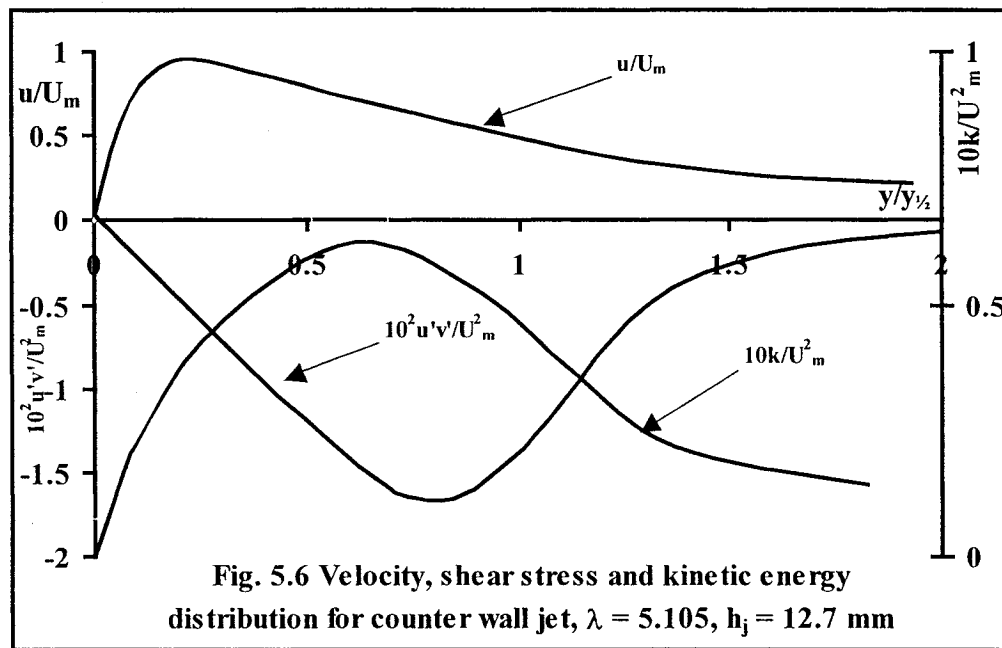


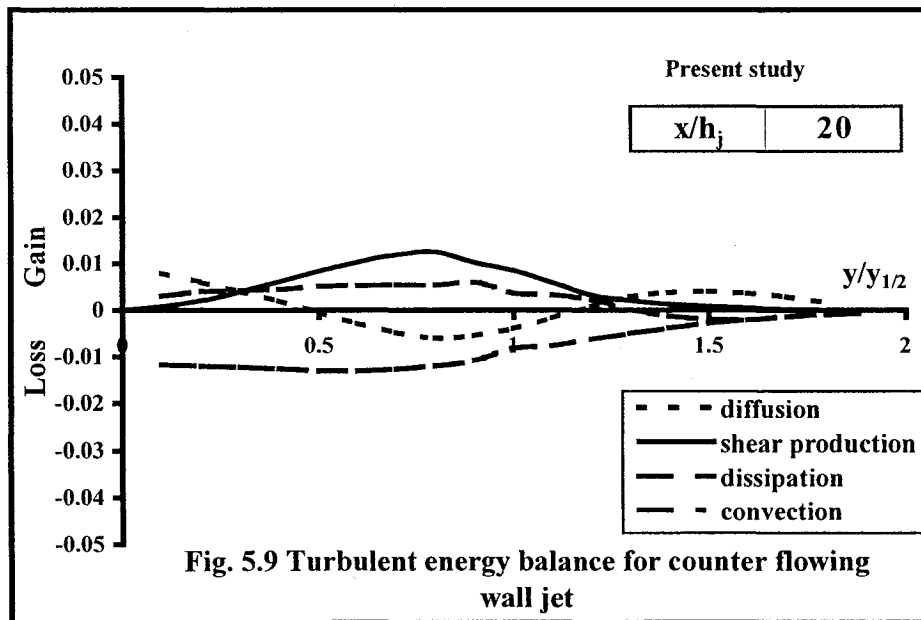
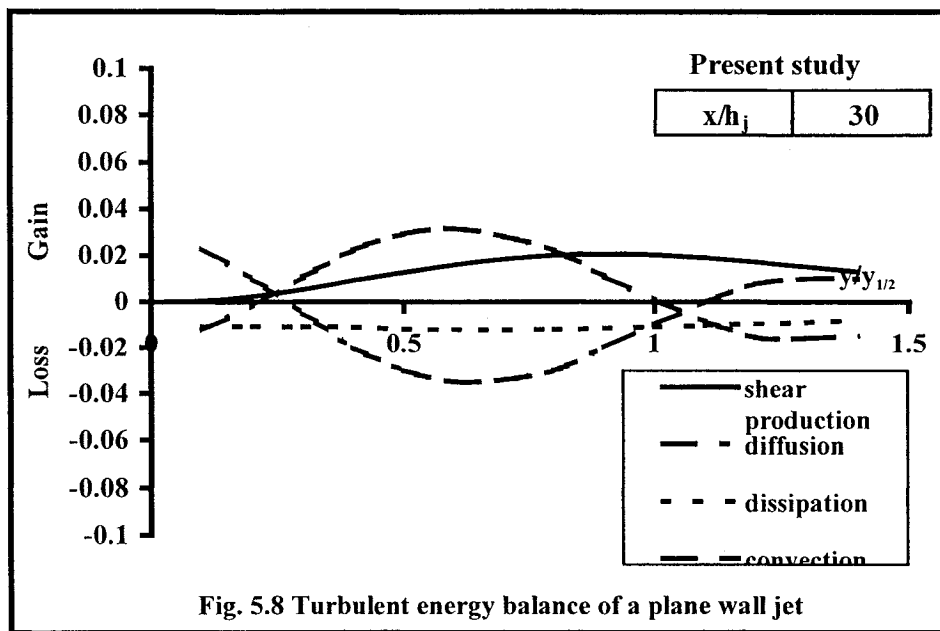












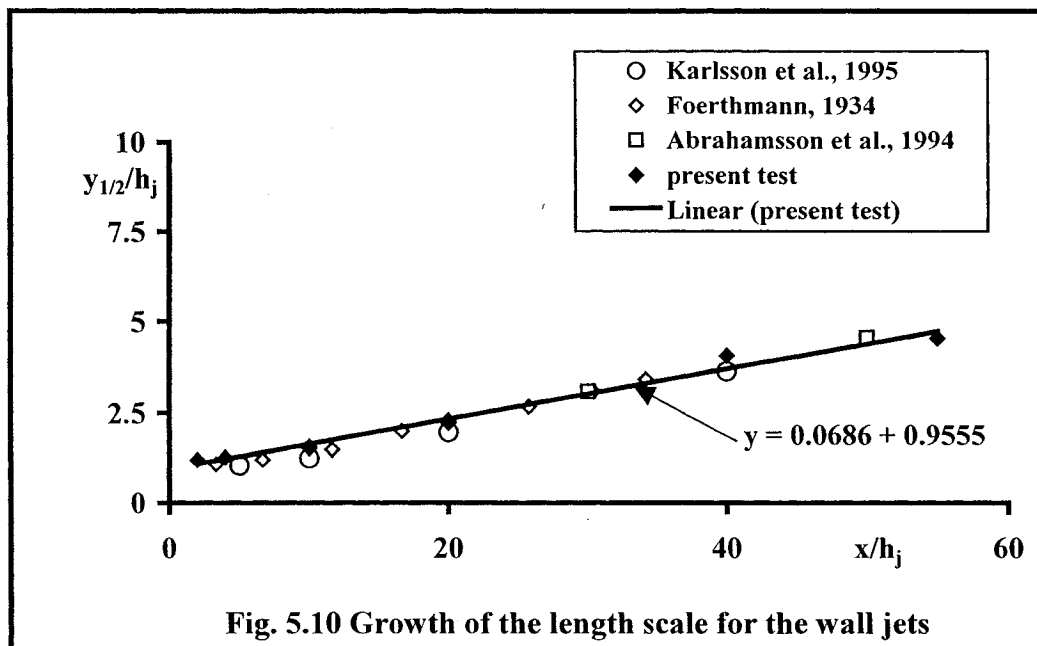


Fig. 5.10 Growth of the length scale for the wall jets

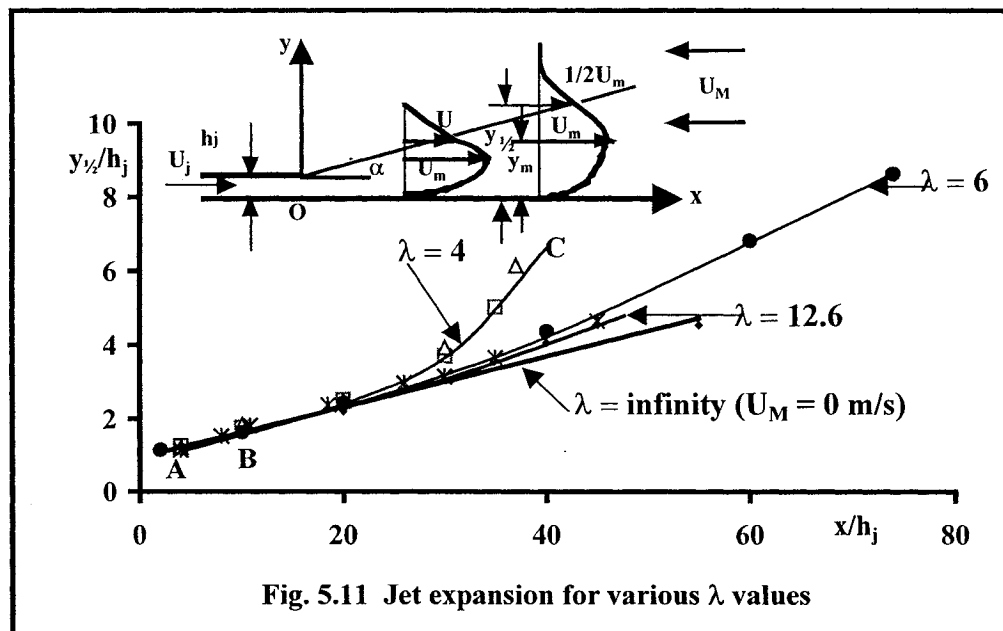
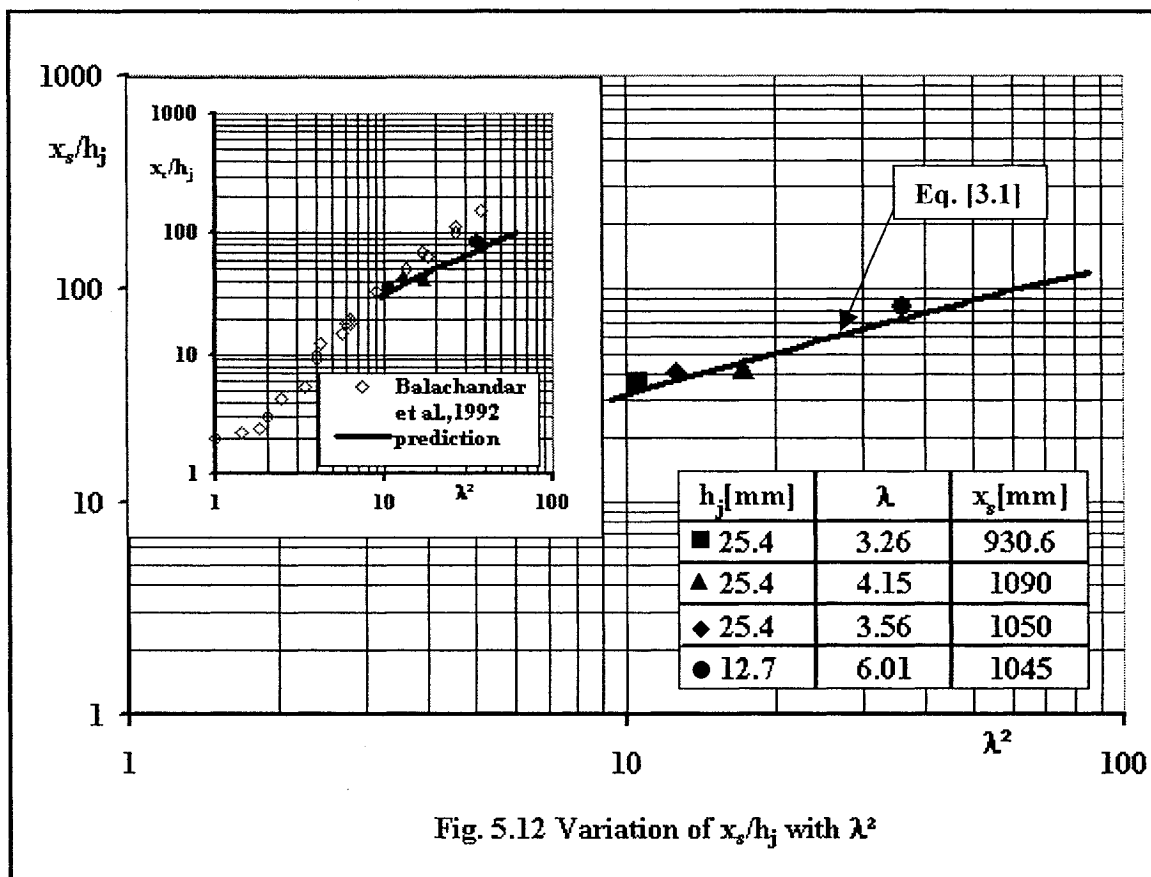
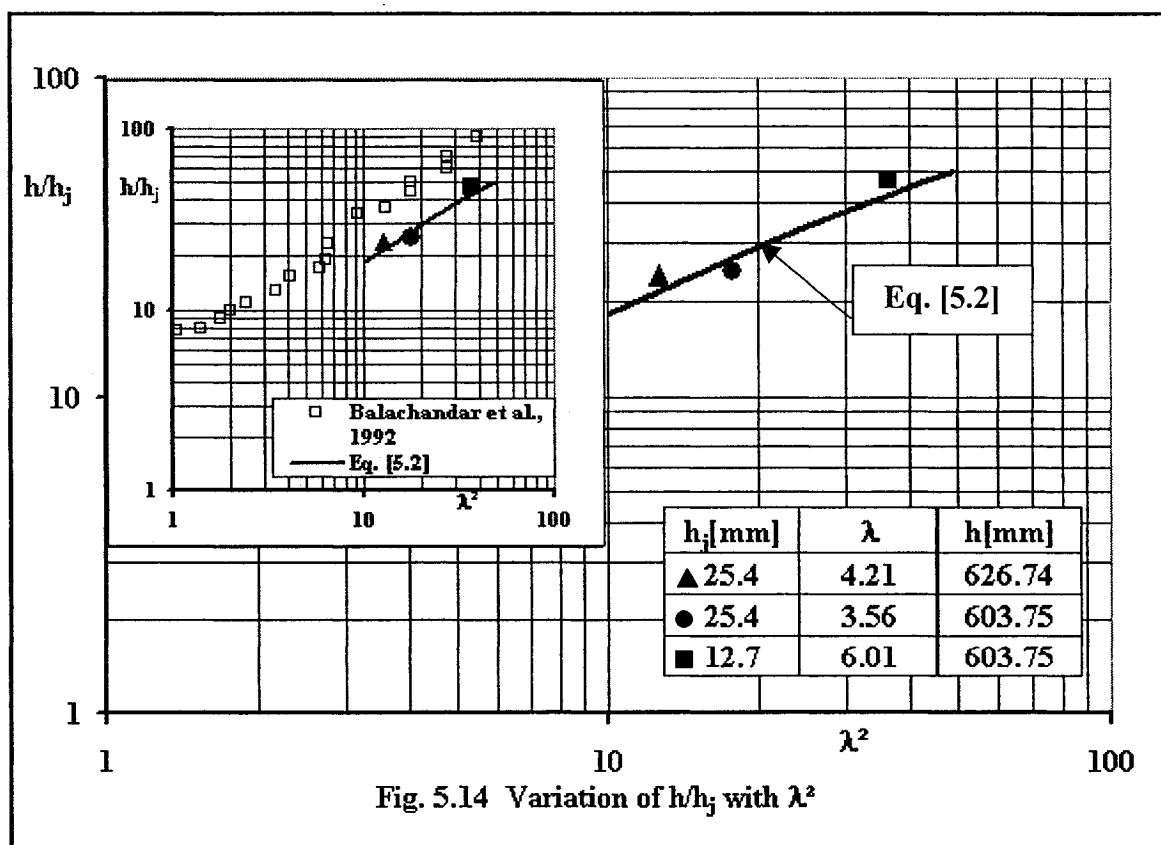
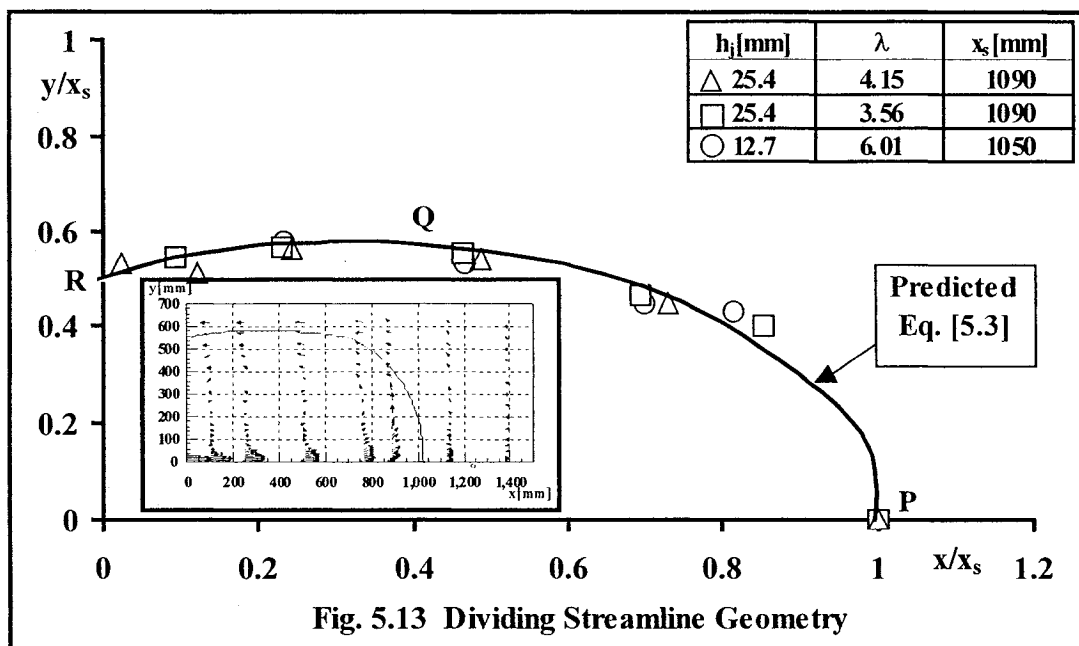
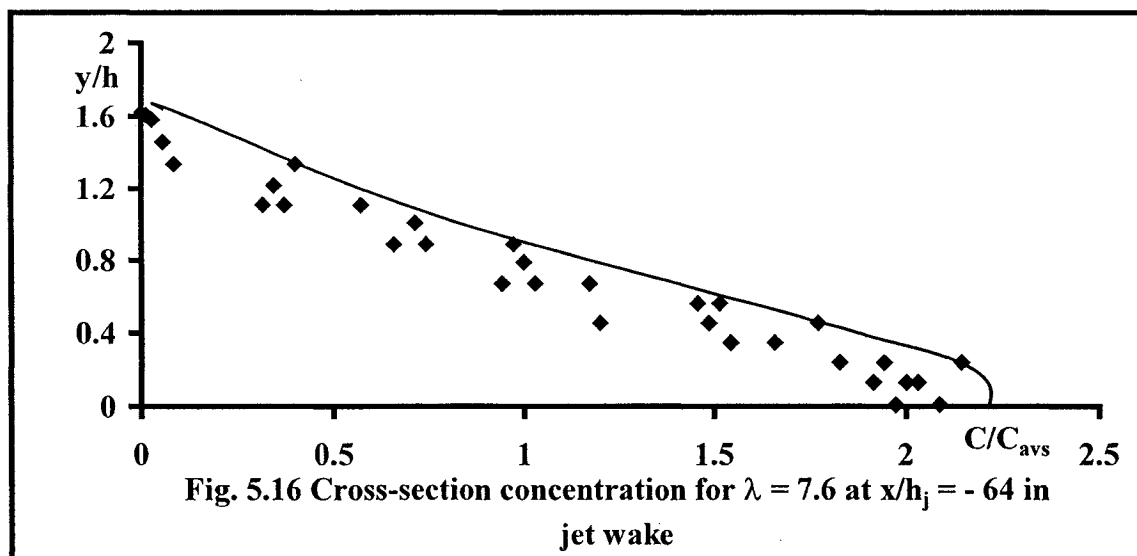
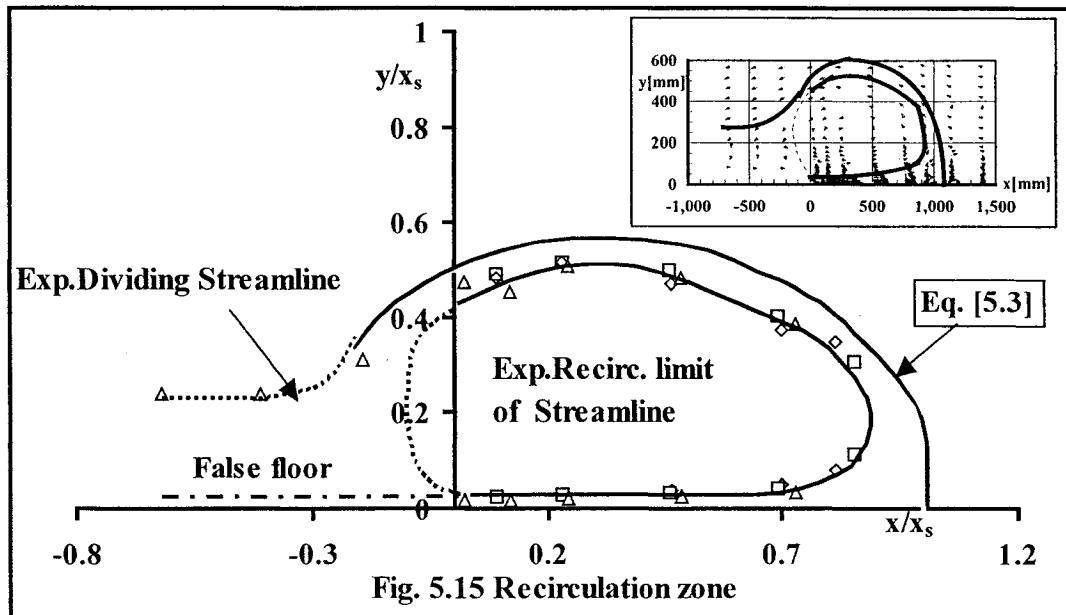
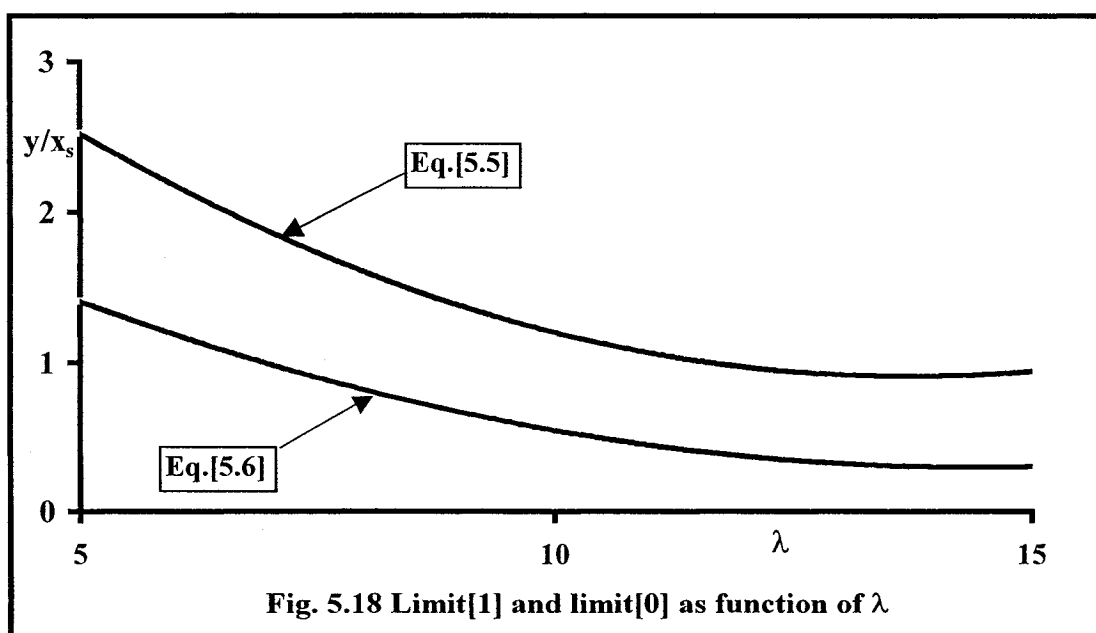
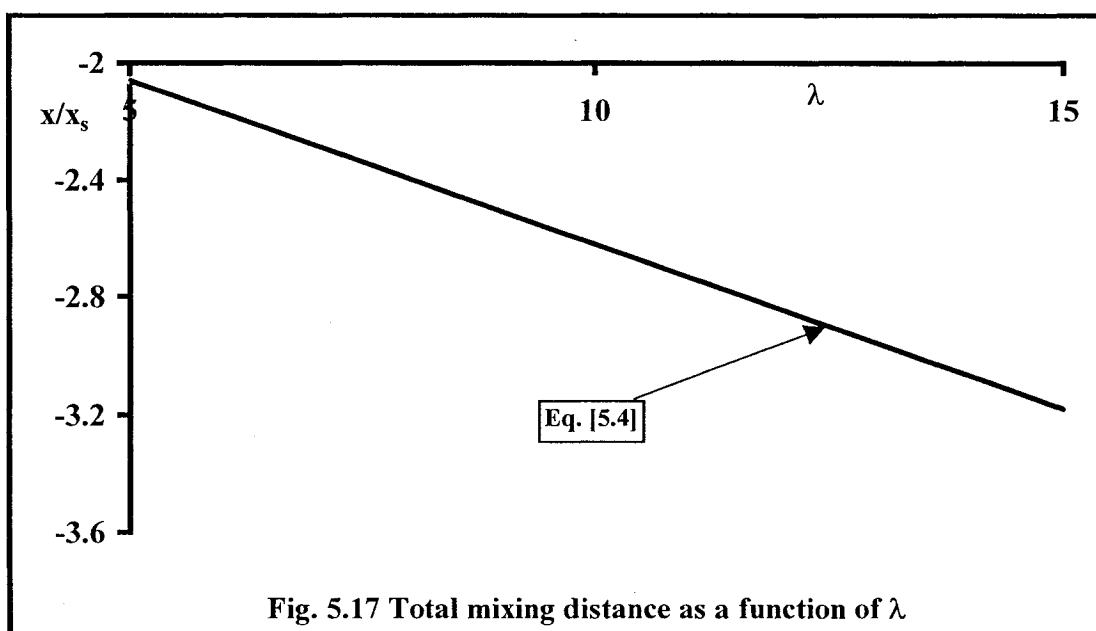


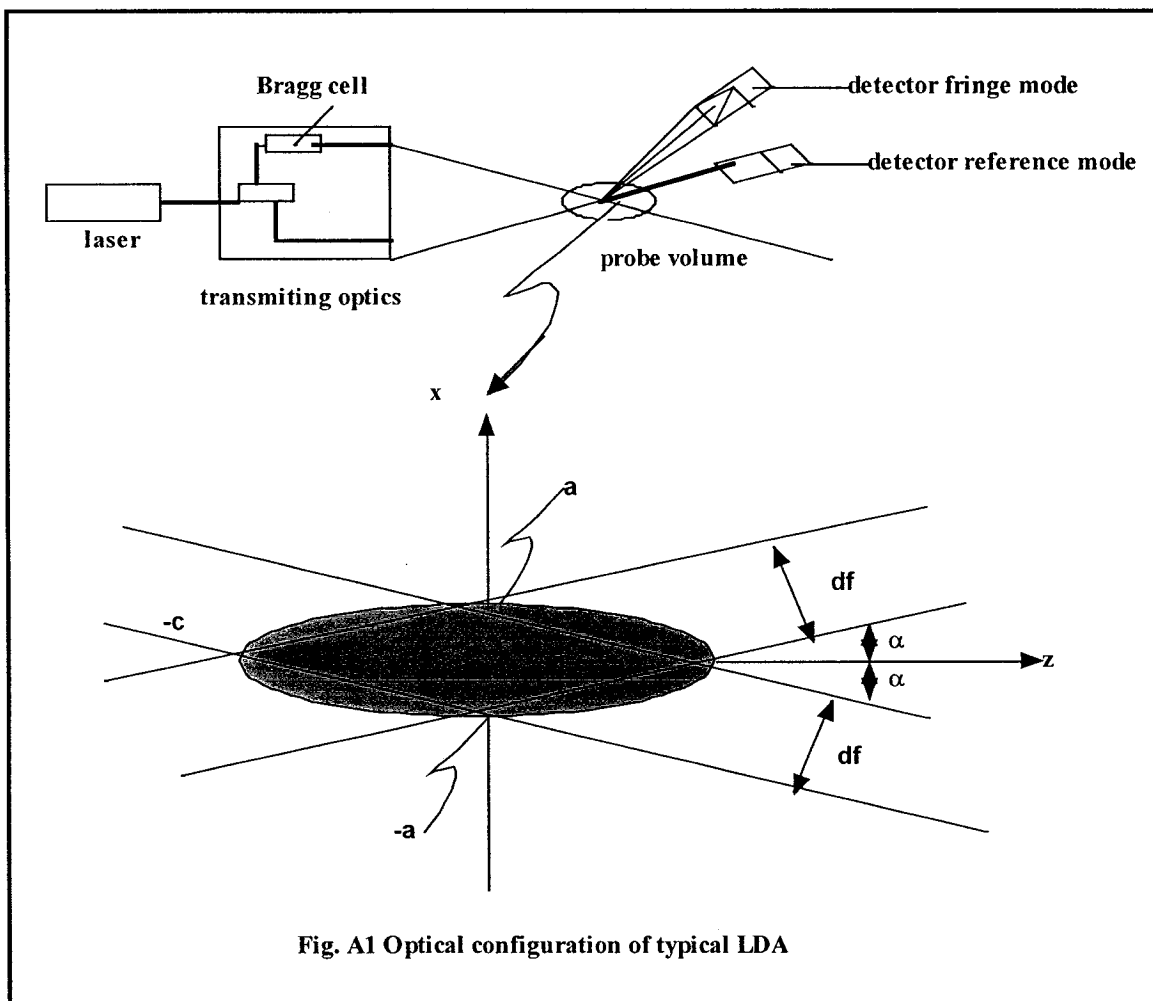
Fig. 5.11 Jet expansion for various  $\lambda$  values



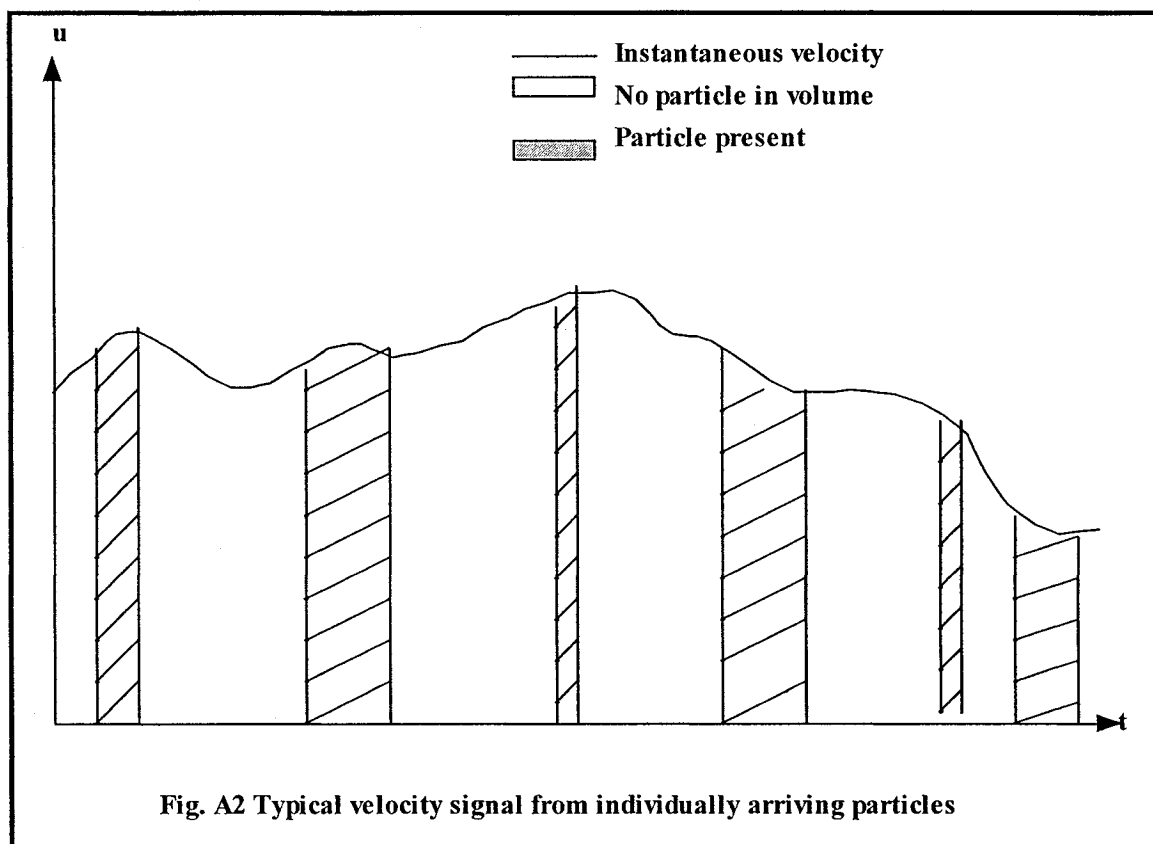












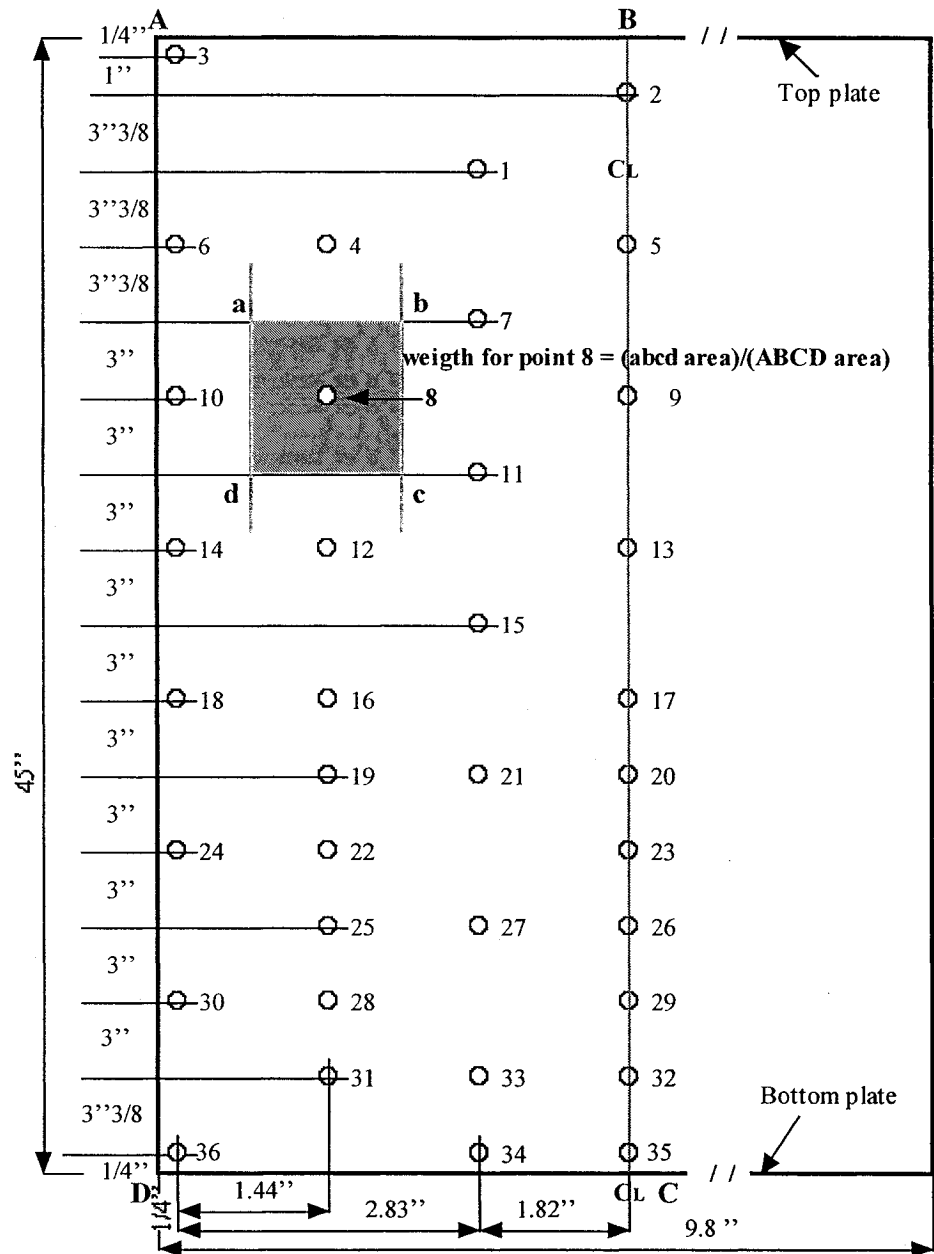


Fig. A3 abcd = area of influence for sampling point 8

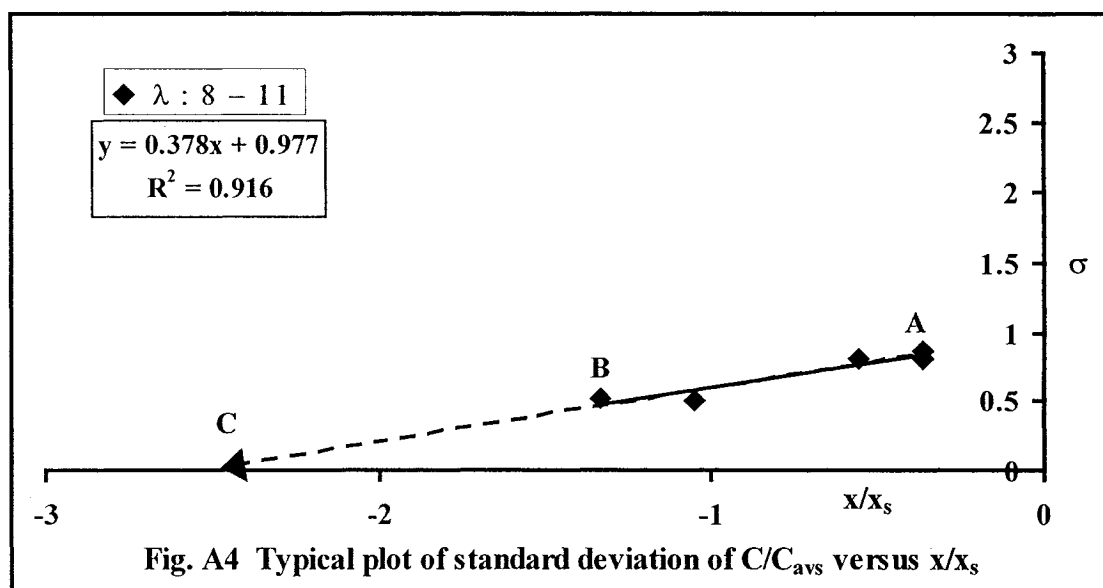


Table 2.1: Wall jets studies

Investigator & Year	$h_j$ [mm]	$10^3 \text{ Re}$	$x/h_j$	Study	Remarks
Förthmann, 1934	30	53	3-33	Experimental	First experimental study of the plane turbulent wall jet based on a theoretical paper of Tollmien (1926). Similarity in the mean velocity profiles for $x$ greater than $20h_j$ .
Glauert, 1956	-----	$10^2$ - $1.4 \times 10^6$	-----	Theoretical	Velocity distribution for both radial and plane wall jet are the same
Sigalla, 1958	7.95	20-50	4-70	Experimental	Measured wall shear stress with Preston probe; The boundary layer thickness varied linearly, at an angle of $3.7^\circ$ with the plate, and passing approximately through the center of the outlet nozzle of the jet.
Bradshaw, 1960	1.02	6.08	339- 1459	Experimental	The first turbulence measurements for 2-d wall jet in still air.
Schwarz, 1960	25.4	22-106	29- 85	Experimental	The location of the virtual origin is a function of the free-stream turbulence in the jet, the wall roughness, vibration, sound, and all the variables, which affect the transition of a laminar flow to a turbulent flow. Each system has its own specific value for the virtual origin and may vary with $Re$ . The angle between the locus of the boundary-layer thickness and the plate was $3.8^\circ$ . No turbulence measurements.
Verhoff, 1963	1.78	10.3 12.1	57- 410	Experimental	The empirical equation that describe the similarity curve of the distribution $u/u_m = 1.48\eta^{1/7} [1 - \text{erf}(0.68\eta)]$ ; No turbulence data.
Mathieu, 1963	6	11-30	33- 200	Experimental	Turbulent characteristics measured for the plane wall jet $u'^2, v'^2, u'v'$ and the distribution of the turbulence production; Reynolds number dependence on the stream wise development of maximum velocity and half-width.
Bradbury, 1965	9.5	-----	-----	Experimental	The structure of a self-preserving turbulent plane jet compared with that of the plane wake.

Investigator & Year	$h_j$ [mm]	$10^{-3} \text{ Re}$	$x/h_j$	Study	Remarks
Rajaratnam, 1967	-----	-----	-----	Theoretical	Observations on the decay of the velocity scale, the average curve being described by the equation $u_m/U_j = 3.5/\sqrt{x/h_j}$ for $x/h_j$ at least up to 100. The virtual origin is located roughly $10b_0$ behind the nozzle, and it is described by the equation $y_{1/2} = 0.068 x$ . Fully developed velocity profiles.
Guillon, 1970	7.62	30.8	26-209	Experimental	
Hanjalić, 1972	-----	-----	-----	Numerical simulation	A model of turbulence – Reynolds stress model – to thin shear flow; the energy balance in wall boundary layer; the velocity and shear stress profiles in plane wall jet with the predictions compared by Tailland & Mathieu's experiment; the energy balance in a plane jet compared with Bradbury's experiment.
Alcaraz, 1977	18	40	20-90	Experimental	The turbulent kinetic energy balance over a convex surface
Ljuboja, 1980	-----	-----	-----	Numerical simulation	Calculated the turbulent wall jets with an algebraic Reynolds stress model (co-flowing and plane wall jet case) as: k- $\epsilon$ , and k- $\omega$ equations.
Lauder, 1981, 1983	-----	-----	-----	Experimental	Claimed that, for the plane two-dimensional wall jet in quiescent surrounding, the linear growth of the half-width was 7.3%, the shear stress was not zero at the point of maximum mean velocity and the interaction of the outer and inner layer attenuated the logarithmic mean velocity profile. The uncertainty of the turbulence data was high, and there was a lack of investigations in well-defined simple geometries.
Chandrsuda, 1981	-----	-----	-----		Studied the terms in the turbulent energy and shear stress balances, for which the turbulent kinetic energy $k = \frac{1}{2} (u^2 + v^2 + w^2)$ was approximated by $k = \frac{3}{4} (u^2 + v^2)$
Kobayashi, 1985	8	17-26	-----	Experimental	$y_{1/2}/h_j = 0.066(x/h_j + 10)$ the growth rate equation; Interesting comparison with free jet turbulence measurements.
Schneider, 1987	5.4	14	43-110	Experimental	$y_{1/2}/h_j = 0.077(x/h_j + 8.7)$ the growth rate equation; LDA captured the Reynolds stress, focusing on the outer most region, were the literature based on hot-wire measurements revealed the largest deviations due to the high local turbulence intensity, and the normal stresses were found to be slightly larger as compared to hot-wire data.

Investigator & Year	$h_j$ [mm]	$10^3 \text{ Re}$	$x/h_j$	Study	Remarks
Fujisawa, 1987	-----	-----	-----	Experimental	Investigated the turbulence energy balance in a two-dimensional wall jet along a plane surface, and found that the convection velocities of the small-scale turbulent motion deviated significantly from the mean velocity. Hot-wire anemometer system
Johansson, 1988	-----	-----	-----	Experimental & Numerical simulation	The energy budget in the near-wall region of the turbulent boundary layer (from experimental data). The classical energy budget from Hinze (2 <sup>nd</sup> Ed., 1975) was poor, compared with the one from DNS (very good).
Karlsson, 1991, 1992, 1993	9.6	9.6	-----	Experimental	Pitot tube and LDV system (the stream wise velocity 488 nm (u), and the normal component 514.5 nm (v)). Measurements stopped at 200 (normalized location) because the flow was losing its wall-jet character.
Abrahamsson 1994	10	10, 15 20	-----	Experimental	Turbulence in a plane two-dimensional wall-jet, employing hot-wire techniques in a large-scale experimental facility; LDA measurements.
Hsiao, 1996	11; 6.7 2.7	3-30	-----	Experimental	Experimental studies on flow transition of a plane wall jet.
Gerodimos, 1997	-----	-----	-----	Numerical simulation	Near wall modeling based on the DNS; four models like k- $\epsilon$ type and k- $\omega$ type for which they obtained a good agreement with other measured quantities. The models reproduced the Reynolds number effects of plane wall jets even their predictions of the jet spread were incorrect.
Eriksson, 1998	As in 1992	9.6	-----	Experimental	Turbulence data from the outer region of the flow compared to earlier hot-wire measurements, and large differences in the normal turbulent intensity and the shear stress were found.
George, 2000	-----	-----	-----	Theoretical	The turbulent plane wall jet without external stream. New theory based on the asymptotic invariance principle (AIP) in which the outer wall jet is governed by different scaling parameters was an excellent agreement with all the experimental data.
Tangermann, 2001	-----	-----	-----	Numerical simulation	Computation of a two-dimensional turbulent wall jet in an external stream. The standard k- $\epsilon$ model and a full Reynolds-stress model has been used for the numerical analysis. A good performance for an engineering point of view has been shown when the region of the negative production of turbulent kinetic energy is small.

Investigator & Year	$h_j$ [mm]	$10^{-3}$ Re	$x/h_j$	Study	Remarks
Tachie, 2002	10	7.5-14	-----	Experimental	LDA measurements in a plane turbulent wall jet. The turbulent wall jet has a universal inner region that is identical to a boundary layer, and the composite velocity profile proposed by the other researchers can be used to model the inner region of the wall jet.

Table 2.2: Counter flowing studies

Investigator & Year	h <sub>j</sub> [mm]	H [mm]	10 <sup>-3</sup> Re	Study	Remarks
Hopkins, 1967	-----	-----	-----	Theoretical	2-d counter flowing jet obtained: the appearance of free streamlines at the sides of the jet and dividing streamline. Kinematic analysis from free-streamline theory and the notched hodograph have been used.
Balachandar, 1992	25.4 6.35 3.13	1524	-----	Experimental	Width of counter flowing wall jet; dividing streamline. Penetration length $x_s$ and wall pressure distributions. The protrusion at jet exit does not disturb flow.
Tanaka, 1994	5	400	6.5 – 19.5	Experimental	Experimental study 2-d wall jet in a turbulent boundary layer. Found streamlines, turbulence intensity contours and static pressure contours for the two typical velocity ratios $\lambda = U_j/U_M$ ( $1 \leq \lambda \leq 3$ ).



Table 5.1 Velocity distribution of plane wall jet

$U_M = 0$	$h_j$ [mm]	12.7	$10^{-3}Re$	19.5
	X [mm]	Y [mm]	U-M[m/s]	V-M[m/s]
	0	0	0.0000	0.0000
	0	2	0.7290	0.0166
	0	3	0.7340	-0.0058
	0	4	0.7400	-0.0143
	0	5	0.7340	-0.0058
	0	6	0.7290	0.0166
	0	7	0.7280	0.0138
	0	12.7	0.0000	0.0000
	25.4	0	0.0000	0.0000
	25.4	2	0.2761	0.0940
	25.4	3	0.5791	0.0135
	25.4	4	0.3542	0.0234
	25.4	5	0.2517	0.0619
	25.4	7.5	0.5432	0.0121
	25.4	10	0.5393	0.0029
	25.4	12.5	0.5249	0.0077
	25.4	15	0.2899	0.0393
	25.4	17.5	0.0972	-0.0046
	25.4	20	0.0372	-0.0146
	25.4	22.5	0.0183	-0.0057
	25.4	25	0.0264	-0.0141
	25.4	30	0.0144	0.0014
	25.4	35	0.0152	-0.0080
	25.4	40	0.0229	-0.0008
	25.4	45	0.0229	0.0010
	25.4	50	0.0018	-0.0157
	25.4	60	0.0080	-0.0135
	25.4	70	0.0223	0.0012
	25.4	80	0.0113	-0.0055
	25.4	90	-0.0002	-0.0042
	25.4	100	-0.0041	-0.0003
	25.4	120	0.0267	0.0650

(Cont'd)

Table 5.1: continued

X [mm]	Y [mm]	U-M[m/s]	V-M[m/s]
25.4	140	0.0323	0.0099
25.4	160	0.0098	0.0027
25.4	180	0.0148	0.0089
127	0	0.0000	0.0000
127	3	0.4905	0.1361
127	4	0.5686	0.0025
127	5	0.5561	0.0014
127	7.5	0.5706	0.0137
127	10	0.5204	0.0281
127	12.5	0.4745	0.0150
127	15	0.4224	0.0039
127	17.5	0.3471	0.0290
127	20	0.2827	0.0234
127	22.5	0.2005	0.0181
127	25	0.1650	0.0365
127	30	0.0636	-0.0189
127	35	0.0123	0.0003
127	40	-0.0025	-0.0106
127	45	-0.0004	-0.0027
127	50	-0.0038	-0.0089
127	60	0.0177	-0.0029
127	70	0.0110	0.0081
127	80	0.0184	-0.0009
127	90	-0.0015	0.0161
127	100	0.0235	0.0038
127	120	0.0143	0.0177
127	140	0.0055	0.0084
127	160	0.0374	0.0153
127	180	0.0229	-0.0032
254	0	0.0000	0.0000
254	2	0.2199	0.1415
254	3	0.4543	0.0109
254	4	0.3982	0.0408
254	5	0.3897	0.0416
254	7.5	0.3069	0.0705

(Cont'd)

Table 5.1: continued

X [mm]	Y [mm]	U-M[m/s]	V-M[m/s]
254	10	0.3552	0.0396
254	12.5	0.3233	0.0418
254	15	0.3123	0.0265
254	17.5	0.3377	0.0466
254	20	0.2618	0.0569
254	22.5	0.2784	0.0560
254	25	0.2454	0.0622
254	30	0.1892	0.0724
254	35	0.1254	0.0373
254	40	0.1006	0.0480
254	45	0.1335	0.0255
254	50	0.0387	0.0082
254	60	0.0283	0.0153
254	70	0.0370	0.0317
254	80	0.0971	0.0389
254	90	0.1838	0.0572
254	100	0.0707	0.0398
254	120	0.0276	0.0171
254	140	0.0891	0.0265
254	160	0.0154	0.0086
254	180	0.0086	-0.0041
508	0	0.0000	0.0000
508	3	0.1668	-0.0011
508	5	0.3385	-0.0023
508	7.5	0.3365	0.0273
508	10	0.3259	0.0159
508	12.5	0.3849	0.0176
508	15	0.3535	0.0005
508	17.5	0.3834	0.0174
508	20	0.2890	-0.0313
508	22.5	0.3195	0.0083
508	25	0.2959	0.0122
508	35	0.3054	-0.0081
508	40	0.2041	0.0162
508	45	0.2369	-0.0155

(Cont'd)

Table 5.1: continued

X [mm]	Y [mm]	U-M[m/s]	V-M[m/s]
508	50	0.2013	0.0487
508	60	0.1454	0.0180
508	70	0.1929	0.0567
508	80	0.1296	0.0784
508	90	0.1164	0.0780
508	100	0.0750	0.0980
508	120	0.1500	0.0802
508	140	0.1260	0.0537
508	160	0.1212	0.0581
508	180	0.1081	0.0262
508	200	0.1219	0.0600
508	220	0.0922	0.0254
698.5	0	0.0000	0.0000
698.5	3	0.1281	0.1241
698.5	5	0.1863	-0.0019
698.5	10	0.2959	-0.0078
698.5	12.5	0.3316	0.0275
698.5	15	0.2814	0.0132
698.5	17.5	0.3019	0.0029
698.5	20	0.3146	0.0037
698.5	22.5	0.2971	0.0191
698.5	25	0.2843	0.0208
698.5	30	0.2411	0.0196
698.5	35	0.2248	0.0094
698.5	40	0.2226	0.0303
698.5	45	0.1849	0.0223
698.5	50	0.1756	0.0158
698.5	60	0.1519	0.0039
698.5	70	0.1134	0.0199
698.5	80	0.1422	0.0108
698.5	90	0.1711	0.0575
698.5	100	0.1465	0.0438
698.5	120	0.0663	0.0257
698.5	140	0.0538	0.0327
698.5	160	0.1061	0.0346

(Cont'd)

Table 5.1: continued

X [mm]	Y [mm]	U-M[m/s]	V-M[m/s]
698.5	180	0.0438	0.0089
889	0	0.0000	0.0000
889	3	0.1974	-0.0582
889	4	0.2070	0.0524
889	5	0.1974	0.0114
889	7.5	0.2536	0.0114
889	10	0.3083	-0.0168
889	12.5	0.2744	0.0444
889	15	0.2082	0.0785
889	17.5	0.2692	0.0587
889	20	0.2386	0.0232
889	22.5	0.1887	0.0343
889	25	0.2582	0.0139
889	30	0.2519	0.0378
889	35	0.1943	0.0790
889	40	0.1939	0.0731
889	45	0.1898	0.0746
889	50	0.1821	0.0663
889	60	0.1402	0.0915
889	70	0.1829	0.0744
889	80	0.1791	0.1066
889	90	0.1762	0.1202
889	100	0.1762	0.0975
889	120	0.1617	0.0895
889	140	0.0987	0.0431
889	160	0.0856	0.0145
889	180	0.1165	0.0355

(Cont'd)

Table 5.2 Velocity distribution of counter flowing wall jet

$\lambda = 5.105$	$h_j[\text{mm}]$	12.7	$10^{-3}\text{Re}$	19.5
	X [mm]	Y [mm]	U-M[m/s]	V-M[m/s]
	-204.47	76.2	0.0000	0.0000
	-204.47	130	0.0263	-0.0915
	-204.47	180	0.0983	-0.0554
	-204.47	220	-0.0820	-0.1069
	-204.47	270	-0.0753	-0.1061
	-204.47	420	-0.1843	-0.0879
	-204.47	470	-0.2086	-0.0909
	-204.47	520	-0.1973	-0.0915
	-204.47	570	-0.2122	-0.0687
	-204.47	620	-0.2107	-0.0582
	-204.47	700	-0.2056	-0.0536
	-204.47	780	-0.1969	-0.0416
	-431.8	76.2	0.0000	0.0000
	-431.8	130	-0.0046	-0.0569
	-431.8	180	0.0023	-0.0919
	-431.8	220	-0.1032	-0.0895
	-431.8	270	-0.0862	-0.0822
	-431.8	320	-0.1462	-0.0766
	-431.8	370	-0.1704	-0.0564
	-431.8	420	-0.1708	-0.0949
	-431.8	470	-0.2008	-0.0815
	-431.8	520	-0.1984	-0.0752
	-431.8	570	-0.1909	-0.0557
	-431.8	620	-0.1916	-0.0395
	-431.8	700	-0.2061	-0.0561
	-431.8	780	-0.2052	-0.0341
	-647.7	82	0.0000	0.0000
	-647.7	130	-0.0346	-0.0858
	-647.7	180	-0.0007	-0.0382
	-647.7	220	-0.1170	-0.0754
	-647.7	270	-0.1424	-0.0868
	-647.7	320	-0.1702	-0.0604
	-647.7	370	-0.1760	-0.0653

(Cont'd)

Table 5.2: continued

X [mm]	Y [mm]	U-M[m/s]	V-M[m/s]
-647.7	420	-0.1920	-0.0607
-647.7	470	-0.1713	-0.0523
-647.7	520	-0.2014	-0.0737
-647.7	570	-0.1813	-0.0417
-647.7	620	-0.1860	-0.0438
-647.7	700	-0.1565	-0.0299
-647.7	780	-0.2058	-0.0385
25.4	0	0.0000	0.0000
25.4	2	0.6217	0.0000
25.4	3	0.8470	0.0000
25.4	4	0.8668	0.0000
25.4	5	0.8548	0.0000
25.4	7.5	0.8882	0.0150
25.4	10	0.8902	0.0092
25.4	12.5	0.7697	0.0247
25.4	15	0.3816	0.0105
25.4	17.5	0.0859	-0.0337
25.4	20	-0.0732	-0.0351
25.4	22.5	-0.1408	-0.0553
25.4	25	-0.1003	-0.0515
25.4	30	-0.0535	-0.0520
25.4	35	-0.0260	-0.0295
25.4	40	0.0577	-0.0983
25.4	45	0.0960	-0.0716
25.4	50	0.1377	-0.0902
25.4	60	0.2129	-0.1284
25.4	70	0.1992	-0.1071
25.4	80	0.2056	-0.0972
25.4	90	0.1799	-0.0891
25.4	100	0.1676	-0.1101
25.4	120	0.2719	-0.0795
25.4	140	0.1446	-0.0647
25.4	160	0.1266	-0.0995
25.4	180	0.1007	-0.1043
25.4	220	0.0614	-0.0661

(Cont'd)

Table 5.2: continued

X [mm]	Y [mm]	U-M[m/s]	V-M[m/s]
25.4	270	-0.0025	-0.1156
25.4	320	-0.1368	-0.0980
25.4	420	-0.1738	-0.0633
25.4	470	-0.1896	-0.0611
25.4	520	-0.2025	-0.0572
25.4	570	-0.1942	-0.0345
25.4	620	-0.1824	-0.0398
25.4	700	-0.2238	-0.0588
25.4	780	-0.1848	-0.0501
127	0	0.0000	0.0000
127	3	0.7507	-0.0042
127	4	0.7889	-0.0033
127	5	0.7385	0.0077
127	7.5	0.7497	-0.0119
127	10	0.7162	0.0038
127	12.5	0.6421	0.0062
127	15	0.5550	-0.0072
127	17.5	0.4995	0.0202
127	20	0.4325	0.0142
127	22.5	0.3114	-0.0045
127	25	0.2545	-0.0118
127	30	0.2234	-0.0147
127	35	0.1846	-0.0142
127	40	0.1260	-0.0153
127	45	0.1553	-0.0299
127	50	0.1404	-0.0217
127	60	0.1491	-0.0342
127	70	0.1458	-0.0510
127	80	0.1268	-0.0384
127	90	0.1599	-0.0712
127	100	0.1460	-0.0543
127	120	0.1222	-0.0505
127	140	0.1351	-0.0783
127	160	0.1246	-0.0610
127	180	0.1237	-0.0290

(Cont'd)



Table 5.2: continued

X [mm]	Y [mm]	U-M[m/s]	V-M[m/s]
127	220	0.0471	-0.0286
127	270	-0.0441	-0.0724
127	320	-0.1110	-0.0633
127	370	-0.1358	-0.0793
127	420	-0.1795	-0.0608
127	470	-0.1901	-0.0368
127	520	-0.2053	-0.0776
127	570	-0.1943	-0.0703
127	620	-0.2030	-0.0643
127	700	-0.2185	-0.0426
127	780	-0.1994	0.0039
254	0	0.0000	0.0000
254	3	0.5302	0.0591
254	4	0.5729	0.0117
254	5	0.6179	0.0140
254	7.5	0.6739	0.0078
254	10	0.6178	0.0024
254	12.5	0.5789	0.0054
254	15	0.5725	0.0201
254	17.5	0.4898	0.0170
254	20	0.4542	-0.0157
254	22.5	0.4805	0.0306
254	25	0.4760	0.0201
254	30	0.3457	0.0053
254	35	0.3090	0.0038
254	40	0.2574	0.0037
254	45	0.2089	-0.0134
254	50	0.1682	-0.0189
254	60	0.1473	-0.0129
254	70	0.1781	-0.0266
254	80	0.1722	-0.0351
254	90	0.1172	-0.0131
254	100	0.2976	0.0166
254	120	0.1609	-0.0424
254	140	0.0844	-0.0213

(Cont'd)

Table 5.2: continued

X [mm]	Y [mm]	U-M[m/s]	V-M[m/s]
254	160	0.0654	-0.0116
254	180	0.0844	-0.0148
254	220	0.0220	-0.0846
254	270	0.0546	0.0197
254	320	-0.0713	-0.0229
254	470	-0.1849	0.0121
254	520	-0.2070	0.0237
254	570	-0.1906	-0.0063
254	620	-0.1966	-0.0411
254	700	-0.1812	-0.0057
254	780	-0.1986	-0.0138
508	0	0.0000	0.0000
508	2	0.5229	0.0220
508	4	0.4959	0.0060
508	5	0.4872	0.0061
508	7.5	0.4753	0.0029
508	10	0.4577	0.0026
508	12.5	0.4629	0.0014
508	15	0.4744	0.0164
508	17.5	0.4615	-0.0060
508	20	0.4368	0.0033
508	22.5	0.4429	-0.0068
508	25	0.4403	0.0135
508	30	0.3726	0.0044
508	35	0.3636	0.0038
508	40	0.3559	0.0081
508	45	0.2977	0.0302
508	50	0.2965	0.0074
508	60	0.2327	0.0043
508	70	0.1653	0.0010
508	80	0.1659	0.0176
508	90	0.1356	0.0134
508	100	0.1403	0.0192
508	120	0.1029	0.0087
508	140	0.1169	0.0203

(Cont'd)

Table 5.2: continued

X [mm]	Y [mm]	U-M[m/s]	V-M[m/s]
508	160	0.1195	0.0239
508	180	0.0816	0.0389
508	220	0.0547	0.0653
508	270	0.0055	0.0827
508	320	-0.0814	0.0488
508	370	-0.1319	0.0614
508	420	-0.1887	0.0464
508	470	-0.1853	0.0591
508	520	-0.1922	0.0847
508	570	-0.1809	-0.0384
508	620	-0.1838	-0.0095
762	0	0.0000	0.0000
762	1	0.1816	-0.1488
762	2	0.3488	0.0039
762	3	0.2495	-0.0072
762	4	0.2823	0.0114
762	5	0.3044	0.0070
762	7.5	0.3240	0.0055
762	10	0.3695	0.0049
762	12.5	0.3522	0.0135
762	15	0.3115	0.0239
762	17.5	0.3451	0.0109
762	20	0.3279	0.0326
762	22.5	0.3406	0.0303
762	25	0.3610	0.0425
762	30	0.3553	0.0259
762	35	0.3075	0.0425
762	40	0.2493	0.0542
762	45	0.3177	0.0805
762	50	0.2872	0.0628
762	60	0.2310	0.0792
762	70	0.2098	0.0442
762	80	0.2080	0.0403
762	90	0.1730	0.0878
762	100	0.1036	0.0344

(Cont'd)

Table 5.2: continued

X [mm]	Y [mm]	U-M[m/s]	V-M[m/s]
762	120	0.1055	0.0378
762	140	0.0679	0.0647
762	160	0.0448	0.0769
762	180	-0.0177	0.0854
762	220	-0.0369	0.0589
762	270	-0.0969	0.1296
762	320	-0.0871	0.1369
762	370	-0.1584	0.1510
762	420	-0.1548	0.1264
762	470	-0.1900	0.0923
762	520	-0.1931	0.0908
762	570	-0.1987	0.0279
762	620	-0.1936	0.0230
939.8	0	0.0000	0.0000
939.8	1	0.0145	0.0007
939.8	3	0.2932	0.0013
939.8	4	0.0254	0.0083
939.8	5	0.0784	0.0123
939.8	7.5	0.2449	0.0089
939.8	10	0.3500	0.0185
939.8	12.5	0.0533	0.0136
939.8	15	0.0337	0.0091
939.8	17.5	0.1057	0.0014
939.8	22.5	0.1130	0.0180
939.8	30	0.2472	0.0271
939.8	35	0.1436	0.0713
939.8	40	0.0941	0.0543
939.8	45	0.0371	0.0422
939.8	50	0.0613	0.0288
939.8	60	0.0164	0.0531
939.8	70	0.0584	0.0589
939.8	80	0.2686	0.1354
939.8	90	0.0384	0.1037
939.8	100	0.2115	0.1352
939.8	140	0.0598	0.1707

(Cont'd)

Table 5.2: continued

X [mm]	Y [mm]	U-M[m/s]	V-M[m/s]
939.8	160	0.0022	0.1984
939.8	180	-0.0303	0.1722
939.8	220	-0.0703	0.1888
939.8	270	-0.1106	0.1670
939.8	320	-0.1582	0.1558
939.8	370	-0.1634	0.1598
939.8	420	-0.1835	0.0719
939.8	470	-0.1935	0.0515
939.8	520	-0.1974	0.1010
939.8	570	-0.2048	0.0827
939.8	620	-0.2031	0.0761
1143	0	0.0000	0.0000
1143	10	0.2914	0.0205
1143	15	0.0199	0.0072
1143	17.5	0.0622	0.0201
1143	20	0.1994	0.0248
1143	22.5	-0.0568	0.0054
1143	25	-0.0748	0.0062
1143	30	0.0671	0.0116
1143	35	-0.0703	0.0104
1143	40	-0.0072	0.0178
1143	45	-0.0203	0.0189
1143	50	0.0930	0.0160
1143	60	0.0586	0.0193
1143	70	-0.0395	0.0111
1143	80	-0.0714	0.0185
1143	90	0.0685	0.0042
1143	100	0.0111	0.0176
1143	120	0.0037	0.0368
1143	140	0.2145	0.0553
1143	160	0.1629	0.0246
1143	180	-0.1022	0.0355
1143	220	-0.0932	0.0444
1143	270	-0.1048	0.0640
1143	320	-0.1232	0.0748

(Cont'd)

Table 5.2: continued

X [mm]	Y [mm]	U-M[m/s]	V-M[m/s]
1143	370	0.0527	0.0992
1143	420	-0.1412	0.0713
1143	470	-0.1468	0.0738
1143	520	-0.1553	0.0637
1143	570	-0.1610	0.0637
1143	620	-0.1636	0.0595
1397	0	0.0000	0.0000
1397	3	-0.0425	0.1050
1397	4	-0.0811	0.0012
1397	5	-0.0299	0.0068
1397	7.5	-0.0810	0.0033
1397	10	-0.0839	0.0104
1397	12.5	-0.0617	0.0058
1397	15	-0.0757	0.0089
1397	17.5	-0.0451	0.0092
1397	20	-0.0753	0.0120
1397	22.5	-0.0909	0.0076
1397	25	-0.0102	0.0126
1397	30	-0.0852	0.0049
1397	35	0.0042	0.0179
1397	40	-0.1020	0.0080
1397	45	-0.0919	0.0127
1397	50	-0.0545	0.0073
1397	60	-0.0094	0.0095
1397	70	-0.0630	0.0202
1397	80	-0.0894	0.0093
1397	90	0.0152	0.0182
1397	100	-0.0489	0.0164
1397	120	-0.0670	0.0164
1397	140	-0.0061	0.0195
1397	160	-0.0826	0.0179
1397	180	-0.1145	0.0167
1397	220	-0.1218	0.0219
1397	270	-0.1219	0.0217
1397	320	-0.1294	0.0259

(Cont'd)

Table 5.2: continued

X [mm]	Y [mm]	U-M[m/s]	V-M[m/s]
1397	370	0.0148	0.0841
1397	420	-0.1363	0.0279
1397	470	-0.1432	0.0316
1397	520	-0.1437	0.0296
1397	570	-0.1437	0.0300
1397	620	-0.1320	0.0296

Table 5.3 Mean velocity profile for a wall jet

$U_M = 0$	$10^{-3}Re$	$x/h_j$	$y_{1/2}[mm]$	$U_m[m/s]$
	25.657	30	89.387	0.8356
	$y/y_{1/2}$	$u/U_m$		
	0.000	0.0000		
	0.034	0.9001		
	0.045	0.8358		
	0.056	0.9968		
	0.084	0.9682		
	0.168	1.0000		
	0.196	0.9367		
	0.224	0.9750		
	0.252	0.9555		
	0.280	0.9842		
	0.336	0.9135		
	0.392	0.8316		
	0.447	0.8636		
	0.503	0.8170		
	0.559	0.7580		
	0.671	0.7820		
	0.895	0.5972		
	1.119	0.3901		

(Cont'd)

Table 5.4b Velocity distribution for  $\lambda = 5.105$ 

$x/h_j$	10	$x/h_j$	20	$x/h_j$	40
$u/U_m$	$y/y_{1/2}$	$u/U_m$	$y/y_{1/2}$	$u/U_m$	$y/y_{1/2}$
0.0000	0.0000	0.0000	0.0000	0.0000	0.0000
0.9516	0.1443	0.7868	0.0962	1.0000	0.1266
1.0000	0.1924	0.8501	0.1282	0.9630	0.1689
0.9361	0.2406	0.9169	0.1603	0.9739	0.2111
0.9503	0.3608	1.0000	0.2404	0.9981	0.2533
0.9078	0.4811	0.9168	0.3206	0.9710	0.2955
0.8139	0.6014	0.8590	0.4007	0.9190	0.3377
0.7035	0.7217	0.8495	0.4809	0.9318	0.3799
0.6332	0.8419	0.7268	0.5610	0.9264	0.4221
0.5482	0.9622	0.6740	0.6412	0.7839	0.5066
0.3947	1.0825	0.7130	0.7213	0.7650	0.5910
0.3226	1.2028	0.7063	0.8015	0.7488	0.6754
0.2832	1.4433	0.5130	0.9618	0.6263	0.7598
0.2340	1.6839	0.4585	1.1221	0.6238	0.8443
0.1597	1.9244	0.3820	1.2824	0.4896	1.0131
		0.3100	1.4427	0.3478	1.1820
		0.2496	1.6030	0.3490	1.3508
		0.2186	1.9236	0.2853	1.5197
				0.2952	1.6885

Table 5.5 Turbulent shear stress profiles for plane wall jet

Present test	$10^{-3}Re$	$x/h_j$
	9.7	20
	$y/y_{1/2}$	$10^2 u'v'/U_m^2$
	0.000	-0.120
	0.102	-0.073
	0.153	-0.008
	0.204	0.079
	0.255	0.183
	0.306	0.298

(Cont'd)



Table 5.5: continued

$y/y_{1/2}$	$10^2 u'v'/U_m^2$
0.357	0.422
0.408	0.549
0.459	0.676
0.612	1.029
0.714	1.213
0.816	1.336
0.918	1.386
1.020	1.358
1.223	1.062

Table 5.6 Mean velocity, shear stress and kinetic energy for counter flowing wall jet

$\lambda$	5.105	$10^{-3} \text{Re}$	19.5	$x/h_j$	20
$y/y_{1/2}$	$u/U_m$	$y/y_{1/2}$	$10^2 u'v'/U_m^2$	$y/y_{1/2}$	$10k/U_m^2$
0.000	0.000	0.000	0.000	0.000	0.000
0.045	0.500	0.200	-0.520	0.100	0.200
0.097	0.790	0.400	-1.000	0.150	0.320
0.150	0.950	0.500	-1.240	0.300	0.460
0.200	1.000	0.600	-1.480	0.450	5.000
0.300	0.970	0.810	-1.780	0.600	0.620
0.350	0.935	1.000	-1.520	0.800	0.580
0.400	0.900	1.100	-1.240	0.900	0.520
0.600	0.750	1.200	-0.920	1.050	0.400
0.750	0.650	1.300	-0.640	1.120	0.350
0.900	0.550	1.400	-0.440	1.200	0.300
1.000	0.500	1.600	-0.240	1.350	0.220
1.150	0.400	1.800	-0.160	1.800	0.140
1.400	0.300	2.000	-0.120		
1.600	0.250				
1.680	0.234				
1.900	0.200				

(Cont'd)

Table 5.7 Turbulent kinetic  
energy for wall jets

Present test	$10^{-3}\text{Re}$	$x/h_j$
	9.7	20
	$y/y_{1/2}$	$k/U_m^2$
	0.000	0.0051
	0.102	0.0111
	0.153	0.0139
	0.204	0.0166
	0.255	0.0191
	0.306	0.0215
	0.357	0.0238
	0.408	0.0259
	0.459	0.0279
	0.612	0.0331
	0.714	0.0359
	0.816	0.0382
	0.918	0.0399
	1.020	0.0411
	1.223	0.0419

(Cont'd)

Table 5.8 Turbulent energy balance of a plane wall jet

$10^{-3}\text{Re}$	25.7	$x/h_i$	30	
$y/y_{1/2}$	Shear Production	Diffusion	Convection	Dissipation
0.000	0.0000			
0.100	0.0004	0.0230	-0.0126	-0.0108
0.200	0.0023	0.0100	-0.0015	-0.0108
0.300	0.0054	-0.0050	0.0106	-0.0110
0.400	0.0092	-0.0200	0.0222	-0.0114
0.500	0.0128	-0.0300	0.0292	-0.0120
0.600	0.0159	-0.0350	0.0314	-0.0123
0.700	0.0184	-0.0340	0.0281	-0.0125
0.800	0.0200	-0.0300	0.0222	-0.0122
0.900	0.0205	-0.0200	0.0111	-0.0116
1.000	0.0202	-0.0100	0.0008	-0.0110
1.100	0.0190	0.0000	-0.0085	-0.0105
1.200	0.0170	0.0080	-0.0155	-0.0095
1.300	0.0150	0.0100	-0.0160	-0.0090
1.400	0.0130	0.0100	-0.0150	-0.0080

(Cont'd)

Table 5.9 Turbulent energy balance terms of counter flowing wall jet

$\lambda$	$10^{-3}\text{Re}$	$x/h_j$		
5.105	19.5	20		
$y/y_{1/2}$	Diffusion	Shear Production	Dissipation	Convection
0.000		0.0000		
0.100	0.0080	0.0008	-0.0118	0.0030
0.200	0.0060	0.0020	-0.0120	0.0040
0.300	0.0040	0.0040	-0.0123	0.0043
0.400	0.0020	0.0062	-0.0126	0.0044
0.500	-0.0005	0.0084	-0.0130	0.0051
0.600	-0.0028	0.0104	-0.0130	0.0054
0.700	-0.0048	0.0120	-0.0127	0.0055
0.800	-0.0060	0.0126	-0.0120	0.0054
0.900	-0.0055	0.0103	-0.0108	0.0061
1.000	-0.0040	0.0086	-0.0083	0.0037
1.100	-0.0017	0.0060	-0.0076	0.0034
1.200	0.0008	0.0032	-0.0063	0.0023
1.300	0.0028	0.0021	-0.0050	0.0002
1.400	0.0038	0.0013	-0.0039	-0.0012
1.500	0.0040	0.0008	-0.0029	-0.0020
1.600	0.0036	0.0004	-0.0020	-0.0020
1.700	0.0028	0.0001	-0.0014	-0.0015
1.800	0.0016	0.0000	-0.0010	-0.0006

Table 5.10 Growth of the length scale for the wall jets

$y_{1/2}/h_j$	$x/h_j$
0.680	0
1.020	5
1.360	10
1.700	15
2.040	20
2.380	25

(Cont'd)

Table 5.10: continued

$y_{1/2}/h_j$	$x/h_j$
2.720	30
3.400	40
4.080	50

Table 5.11 Jet expansion

$U_M = 0$	$y_{1/2}/h_j$	$x/h_j$	$\lambda = 4$	$y_{1/2}/h_j$	$x/h_j$
	0	0.680		4	1.261
	5	1.020		4	1.226
	10	1.360		10	1.762
	15	1.700		10	1.841
	20	2.040		20	2.527
	25	2.380		20	2.483
	30	2.720		30	3.712
	40	3.400		30	3.930
	50	4.080		35	5.024
			37	6.139	

$\lambda = 6$	$y_{1/2}/h_j$	$x/h_j$	$\lambda = 12.6$	$y_{1/2}/h_j$	$x/h_j$
	2	1.149		4	1.151
	10	1.637		8	1.535
	20	2.456		10.8	1.818
	40	4.370		18.5	2.391
	60	6.822		26	2.986
	74	8.632		30	3.156
				35	3.662
			45	4.653	

(Cont'd)

Table 5.12 Variation of  
 $x_s/h_j$  with  $\lambda^2$

$h_j$ [mm]	$\lambda$	$x_s$ [mm]
25.4	3.26	930.6
25.4	4.15	1090
25.4	3.56	1050
12.7	6.01	1045

Table 5.13 Dividing Streamline Geometry

$h_j$	$\lambda$	$x_s$	$x/x_s$	$y/x_s$
25.4	4.15	1090	0.09321	0.54303
			0.23303	0.57798
			0.46606	0.53275
			0.69908	0.44708
			0.8156	0.43207
			1	0
25.4	3.56	1050	0.09234	0.54274
			0.23085	0.56347
			0.4617	0.55345
			0.69255	0.46462
			0.85414	0.40285
			1	0
12.7	6.01	1050	0.02431	0.52981
			0.12153	0.50873
			0.24306	0.56215
			0.48612	0.54067
			0.72919	0.44706
			1	0

(Cont'd)

Table 5.14 Variation of  $h/h_j$   
with  $\lambda^2$

$h_j[\text{mm}]$	$\lambda$	$h[\text{mm}]$
25.4	4.21	626.7
25.4	3.56	603.8
12.7	6.01	603.8

Table 5.15 Recirculation zone

$h_j [\text{mm}]$	$\lambda$	$x_s[\text{mm}]$	$x/x_s$	$y/x_s$
25.4	4.15	1090	0.09321	0.48234
			0.23303	0.51661
			0.46606	0.46879
			0.69908	0.37368
			0.8156	0.35021
25.4	3.56	1050	0.09234	0.48973
			0.23085	0.51597
			0.4617	0.4982
			0.69255	0.40338
			0.85414	0.30816
12.7	6.01	1050	0.02431	0.47662
			0.12153	0.45572
			0.24306	0.50888
			0.48612	0.48453
			0.72919	0.38455
			-0.1957	0.31266
			-0.6198	0.23901
			-0.4132	0.23781

(Cont'd)

Table 5.16 Cross-section concentration  
for  $\lambda=7.6$  at  $x/h_j = -64$

h <sub>j</sub> [mm]	12.7	y/h	C/C <sub>avs</sub>
x <sub>s</sub> [mm]	1221.866	1.460	0.057
h[mm]	702.573	1.582	0.029
		1.604	0.014
		1.618	0.000
		1.582	0.029
		1.338	0.086
		1.338	0.086
		1.338	0.400
		1.216	0.343
		1.107	0.372
		1.107	0.572
		1.107	0.314
		1.008	0.715
		0.890	0.743
		0.890	0.972
		0.890	0.658
		0.791	1.001
		0.673	1.029
		0.673	1.172
		0.673	0.943
		0.565	1.515
		0.565	1.458
		0.565	1.515
		0.456	1.487
		0.456	1.773
		0.456	1.201
		0.348	1.658
		0.348	1.544
		0.348	1.544
		0.240	2.144
		0.240	1.830
		0.240	1.944
		0.131	2.030

(Cont'd)



Table 5.16: continued

$y/h$	$C/C_{\text{avs}}$
0.131	1.915
0.131	2.001
0.009	1.973
0.009	2.087
0.009	1.973
0.009	1.973

Table A4:  $\sigma$  versus  $x/x_s$ 

$x/x_s$	$\sigma$	$\lambda$
-0.353	0.67	7.6
-0.530	0.56	7.6
-0.530	0.60	7.6
-0.665	0.56	7.6
-1.640	0.59	5.6
-2.088	0.62	5.6
-0.208	0.79	10.9
-0.360	0.80	10.9
-0.360	0.87	10.9
-0.554	0.80	10.9
-1.048	0.51	8.2
-1.334	0.51	8.2
-0.152	0.89	14.5
-0.264	1.02	14.5
-0.407	1.02	14.5
-0.794	0.82	10.5
-0.794	0.93	10.5
-1.011	0.95	10.5